Spherical Lumps in the Cosmic Custard

A Search for the Parameters of
Effective Field Theory of Large Scale Structures
in Spherical Collapse

Thesis for the master's programme Theoretical Physics

by

Nikki Bisschop

Supervisor **Dr. Enrico Pajer**

Institute for Theoretical Physics
Utrecht University

Universiteit Utrecht

Preface

The master's programme *Theoretical Physics* at Utrecht University consists of two major parts. The first part consists of the obligatory courses in quantum and statistical field theory, and optional courses varying from soft-condensed matter theory to string theory. The other part is the master's research project.

After finishing most of the due courses I started looking for a research project. Following the course on cosmology by Tomislav Prokopec gained my interest in cosmology. In the summer of 2014 Enrico Pajer came from Princeton to Utrecht. When I dropped by his office he told me very enthusiastically that the research field of large scale structures was where it was happening right now in cosmology. As it just happened to be, this was exactly his discipline.

His compelling story convinced me to ask him to supervise my master's research and I was very pleased he said yes. One week earlier Stella Boeschoten, another master's student, started with her research under the supervision of Dr. Pajer as well. Because we both had to familiarize ourselves with the most important parts of the theory of large scale structures, we collaborated and had meetings with the three of us.

First, we had the plan to diverge our research once we would arrive at the first milestone on our roadmap. Unfortunately, the learning curve was steep and we never got past that first milestone, so we kept collaborating all year long, culminating in a combined presentation for the staff and students of the Institute for Theoretical Physics of Utrecht University on June 25th, 2015.

During this year I have learned a lot about large scale structures and cosmology in general. Moreover this year gave a great insight in how one conducts scientific research. I would like to thank all members of the cosmology group and especially Enrico Pajer and Stella Boeschoten for this valuable experience.

Nikki Bisschop

Contents

Notation and Conventions

Integrals

$$\int_{\boldsymbol{x}} \equiv \int \mathrm{d}^3 x \qquad\qquad \int_{\boldsymbol{k}} \equiv \int \frac{\mathrm{d}^3 k}{(2\pi)^3}$$

$$\int_{\boldsymbol{x}'} \delta_D(\boldsymbol{x}-\boldsymbol{x}')f(\boldsymbol{x}') \equiv f(\boldsymbol{x}) \qquad\qquad \int_{\boldsymbol{k}'} \delta_D(\boldsymbol{k}-\boldsymbol{k}')f(\boldsymbol{k}') \equiv f(\boldsymbol{k})$$

Fourier Transform

$$f(\boldsymbol{x}) \equiv \int_{\boldsymbol{k}} f(\boldsymbol{k}) \mathrm{e}^{-\mathrm{i}\boldsymbol{k}\cdot\boldsymbol{x}} \qquad\qquad f(\boldsymbol{k}) \equiv \int_{\boldsymbol{k}} f(\boldsymbol{x}) \mathrm{e}^{\mathrm{i}\boldsymbol{k}\cdot\boldsymbol{x}}$$

Variables and fields

$\boldsymbol{x}$	$= a\boldsymbol{r}$	Comoving position in real space
$\boldsymbol{v}(\boldsymbol{x},\tau)$	$= \dfrac{\mathrm{d}x}{\mathrm{d}\tau}$	Peculiar velocity
$\rho(\boldsymbol{x},\tau)$		Local density
$\bar{\rho}(\tau)$		Background density
$\delta(\boldsymbol{x},\tau)$	$= \rho(\boldsymbol{x},\tau)/\bar{\rho}(\tau) - 1$	Local density contrast
$\theta(\boldsymbol{x},\tau)$	$= \nabla \cdot \boldsymbol{v}(\boldsymbol{x},\tau)$	Velocity divergence
$\Phi(\boldsymbol{x},\tau)$		Cosmological gravitational potential

Chapter 1

Introduction

Looking up the night's sky has been a popular pastime in the entire history of humankind, always asking what was up there and how we ended down here. First, they saw signs in the arrangements of the stars and planets. That inspired many to minutely keep track of all the objects seen at night. Later came the realization that all those stars were just similar to our sun, that there were planets similar to ours revolving around those stars, and that what we called the Milky Way was just one of many galaxies.

During the centuries we became ever more aware that Earth is not a special place in the Universe, yet it is still fascinating to look into the sky and wonder how everything came into being. Using ever more advanced instruments, from the naked eye to unmanned space telescopes, we managed to look deeper and deeper into space, and thus back in time. It was in 1964 that Arno Penzias and Robert Wilson were experimenting with a horn antenna, originally designed to pick up communication signals, that there was this one signal coming from every direction they could not put their finger on. It was not caused by some pigeons nesting in their equipment, instead it was the oldest electromagnetic signal, the cosmic microwave background radiation (CMBR) – not surprisingly later coined the baby picture of the Universe.

From this baby picture we have learned that the Universe is extremely isotropic, the anisotropies are only in the order 10^-5. Since the beginning of the twentieth century the homogeneity of the Universe, known as the Cosmological Principle, was already assumed; the CMBR strengthened the believe in this assumptions. Later red-shift surveys, which can give a three dimensional picture of the density distribution really proved that the Universe was homogeneous on large scales, scales larger than approximately 100 Mpc (the Local Group, the group of around 50 galaxies we reside in, has an approximate diameter of 3.1 Mpc).

At the same time, we know that on smaller scales the inhomogeneities are very big. This is all a natural result of how the Universe evolved. The leading narrative now is that after the Big Bang there was a very short time of inflation, not longer than 10^{-32} seconds. That is the explanation for the homogeneity of regions of the Universe that seem to be otherwise causally disconnected. After that very brief inflation epoch, radiation dominated up to 70,000 years after the Big Bang. From that time matter started to dominate the energy density of the Universe for most of the time up to now. Now, most of the energy density can be attributed to dark energy.

What the origins of this dark energy are, remains one of the big questions of Cosmology. The most widely used model is the ΛCDM model which assumes this density to be constant, therefore its importance grows as the Universe expands and the matter and radiation content dilutes. At the present time it makes up about 70 % of the entire energy density and it is responsible for the accelerating expansion of the Universe. Only about one fifth of the final 30 % is baryonic matter, which leaves approximately 25 % of the entire energy density to be what we call dark matter. We know that this matter interacts with ordinary baryonic matter through gravity and that other interactions with this matter are, if present at all, very weak. Many researchers, cosmologists as well as particle physicists, are currently trying to find a good explanation for the dark matter content.

Another big question is where the asymmetry between matter and anti-matter comes from. From the standard model of particle physics one would assume there would be equal amounts of baryons and anti-baryons, but now we see practically only matter and virtually no anti-matter. One explanation would be that the Universe is divided in different regions where either matter or anti-matter dominates. That leads us directly to the problem of how the matter and anti-matter gets separated enough such that it does not annihilate. One possibility would be that gravity does not work equally on anti-matter as on matter particles, but this would violate general relativity. All those ideas are highly speculative and there is not yet any experimental (dis)proof for them.

We leave all those question aside and take a look at how the matter content is distributed in the Universe. On the large scales it is almost perfectly homogeneous and we allot this to almost homogeneous initial conditions. The tiny inhomogeneities in this initial conditions are thought to be caused by quantum fluctuations right after the big bang and to be stretched by inflation. There are many competing theories to explain inflation, and they all have a different effect on these so-called primordial perturbations. Therefore measuring the primordial perturbations tells us something about the mechanism behind inflation.

After inflation and the radiation epoch, matter starts to dominate. The pressure drops and gravity starts to dominate the large scales. Gravitational pull towards overdense regions is larger and attracting more and more matter makes them more overdense. In chapter 2 we will first explore the dynamics of the density perturbations on large scales. We will derive the equations of motion from Newtonian physics and the expansion of the Universe. It turns out that the matter distribution is acting as a pressureless fluid. Because the density only deviates slightly from the average density, we will use perturbation theory (section 2.2) to find solutions for these equations of motion.

Perturbation theory however demands that the expansion parameter is small in any regime. Although the density contrast stays small on the very large scales, on small scales it becomes extremely non-linear. Because the difference between those scales – the observable Universe has an approximate diameter of 28 Gpc while the typical scale for structure formation is only 10 Mpc – is gigantic, it still works reasonably well on those large scales, but as experimental research progresses we can no longer sweep these small scale perturbations under the carpet and pretend they are not there.

However, we are also not really interested in what exactly happens on the small scales, we only want to know what the effects are on the large scales. That is exactly what Effective Field Theory is all about, it reduces short-scale physics to some parameters in the long-scale equations of motion. In chapter 3 we will look for those parameters in large scale structure formation. Just like in ordinary fluids we get the effective pressure, the speed of sound and the viscosity of the Universe. By design they cancel the UV-divergences that otherwise arise and we checked they really do.

The values of the parameters of the Effective Field Theory of Large Scale Structures (EFTofLSS) can be obtained from measurements or N-body simulations, but not from the theory itself. An analytical result would provide us more intuitive insight in the effective theory. To obtain an analytical value for the effective parameters we will look at the special case of spherical collapse in chapter 4. Unfortunately there is no final result of our search for these parameters in this specific case in this thesis, but we took some first steps in the right direction and will point out in chapter 6 what steps are left.

The hope is that eventually it is possible to divide the entire cosmic web into parts that have different symmetries. One of those building blocks would then be the spherical collapse solution, others would be linear collapse resulting in cosmic walls and cylindrical collapse which results in filaments.

All these structures are observed by red-shift surveys. Large Scale Structures is a very active research field and there are many projects pushing the boundaries on the measurements. In chapter 5 we will briefly review what measurements are done right now and what we can expect in the (near) future.

Chapter 2

Evolution of Large Scale Structures

One can derive from the CMB that in the early Universe the matter distribution was very isotropic and homogeneous, with maximal perturbations of the order 10^{-5}. In a sea of particles, matter perturbations tend to grow, no matter how small they start. There are two effects of inhomogeneities on an individual particle. First there is the pressure which provides a force away from overdensities. Gravity on the other hand is attractive and thus points in the opposite direction.

These two forces, pressure and gravity, are therefore responsible for the evolution of inhomogeneities: overdensities grow there where gravity is stronger than pressure, while they fade out if the pressure is stronger. In early times, when the Universe was much smaller, pressure was stronger than gravity, and therefore inhomogeneities were not growing. While the Universe expanded, the gravity took over and matter started to cluster. If however the Universe would expand very rapidly, the dilution of the densities could make the matter collapse impossible.

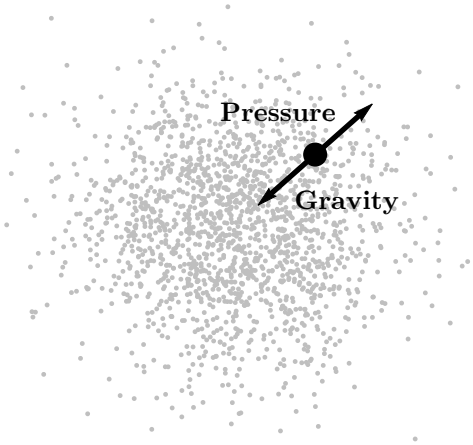

Figure 2.1: Pressure lets overdensities decrease, while the attractive gravitational force lets overdensities increase and small inhomogeneities turn into grow into structures.

Though on large scales the Universe is still very homogeneous, the formation of structures resulted in very large inhomogeneities on smaller scales. Compare for example the density of a galaxy and that of the space between clusters.

In 2001 Bernardeau *et al.*[1] reviewed the formalism and application of perturbation theory in large scale structures. We closely follow their work that set a standard here.

2.1 The Equations of Motion

When looking at large scale structures, our aim is to find a description of the density as a function of space and time. The largest part of the matter density in the universe consists of dark matter, so we will start by imagining a sea of particles only interacting gravitationally. The remaining, baryonic matter follows the dark matter distribution, so this will give us a good description of the total matter density distribution.

The motion of a single particle with mass m at position $\boldsymbol{r}$, with velocity $\boldsymbol{u}$ surrounded by particles with mass m_i at positions $\boldsymbol{r}_i$ is given by the Newtonian equation

$$\frac{\mathrm{d}\boldsymbol{u}}{\mathrm{d}t} = G_\mathrm{N} \sum_i \frac{\boldsymbol{r}_i - \boldsymbol{r}}{|\boldsymbol{r}_i - \boldsymbol{r}|^3} m_i.$$

Because we are interested in large scales where great numbers of particles interact, we take the continuum limit,

$$\frac{\mathrm{d}\boldsymbol{u}}{\mathrm{d}t} = G_\mathrm{N} \int \mathrm{d}^3 r' \, \rho(\boldsymbol{r}') \frac{\boldsymbol{r}' - \boldsymbol{r}}{|\boldsymbol{r}' - \boldsymbol{r}|^3} \equiv -\frac{\mathrm{d}\phi(\boldsymbol{r})}{\mathrm{d}\boldsymbol{r}}, \tag{2.1}$$

with $\rho(\boldsymbol{r}, t)$ the matter density and the resulting gravitational potential given by,

$$\phi(\boldsymbol{r}) = G_\mathrm{N} \int \mathrm{d}^3 r' \, \frac{\rho(\boldsymbol{r}')}{|\boldsymbol{r}' - \boldsymbol{r}|}$$

Because the Universe is on large scales homogeneous and isotropic, we assume a Friedman-Lemaître-Robertson-Walker (FLRW) metric, $g_{\mu\nu} = a(t)\,\mathrm{diag}(-1, 1, 1, 1)$, with $a(t)$ the scale factor. We define conformal time τ by $\mathrm{d}t = a(\tau)\,\mathrm{d}\tau$ and define the comoving coordinates $\boldsymbol{x} = a^{-1}\boldsymbol{r}$. In a perfectly homogeneous expanding Universe, all particles would move with the Hubble flow, we want to describe the deviations from that, therefore we define the peculiar velocity,

$$\boldsymbol{v} \equiv \frac{\mathrm{d}\boldsymbol{x}}{\mathrm{d}\tau} = \boldsymbol{u} - \mathcal{H}\boldsymbol{x}, \qquad \text{with the comoving Hubble flow } \mathcal{H} \equiv \frac{1}{a}\frac{\mathrm{d}a}{\mathrm{d}\tau}.$$

Also for the densities, we just want to describe the deviations from the homogeneous background. Therefore we define the density contrast,

$$\rho(\boldsymbol{x}, \tau) = (1 + \delta(\boldsymbol{x}, \tau))\bar{\rho}(\tau),$$

which leads together with the Friedmann equations to the Poisson equation,

$$\nabla^2 \Phi(\boldsymbol{x}, \tau) = \frac{3}{2}\Omega_m \mathcal{H}^2 \delta(\boldsymbol{x}, \tau), \tag{2.2}$$

for the cosmological gravitational potential,

$$\Phi = \phi + \frac{1}{2}\frac{\mathrm{d}\mathcal{H}}{\mathrm{d}\tau} x^2.$$

The distribution of matter in the Universe can be described by the density distribution function $f(\boldsymbol{x}, \boldsymbol{v}, \tau)$. Phase-space conservation for this function implies the Vlasov equation

$$\frac{\mathrm{d}}{\mathrm{d}\tau} f(\boldsymbol{x}, \boldsymbol{v}, \tau) = \frac{\partial}{\partial \tau} f(\boldsymbol{x}, \boldsymbol{v}, \tau) + \boldsymbol{v} \cdot \frac{\partial}{\partial \boldsymbol{x}} f(\boldsymbol{x}, \boldsymbol{v}, \tau) - (\nabla\Phi + \mathcal{H}\boldsymbol{v}) \frac{\partial}{\partial \boldsymbol{v}} f(\boldsymbol{x}, \boldsymbol{v}, \tau) = 0. \tag{2.3}$$

This equation is obviously very hard to solve. Because we are interested in the time evolution of the spatial distribution only, we will integrate out the momentum, which is done by taking moments. The zeroth moment is simply the density,

$$\int \mathrm{d}^3 v \, f(\boldsymbol{x}, \boldsymbol{v}, \tau) = \rho(\boldsymbol{x}, \tau). \tag{2.4}$$

The first and second moment are then defined as,

$$\int \mathrm{d}^3v\, \boldsymbol{v} f(\boldsymbol{x},\boldsymbol{v},\tau) = \rho(\boldsymbol{x},\tau)\boldsymbol{v}(\boldsymbol{x},\tau) \tag{2.5}$$

$$\int \mathrm{d}^3v\, v^i v^j f(\boldsymbol{x},\boldsymbol{v},\tau) = \rho(\boldsymbol{x},\tau)v^i(\boldsymbol{x},\tau)v^j(\boldsymbol{x},\tau) + \sigma^{ij}(\boldsymbol{x},\tau) \tag{2.6}$$

We see that for every additional moment we need an additional variable. Now we take the zeroth moment of the Vlasov equation and find the so called continuity equation,

$$\partial_\tau \delta(\boldsymbol{x},\tau) + \nabla\left[(1+\delta(\boldsymbol{x},\tau))\,\boldsymbol{v}(\boldsymbol{x},\tau)\right] = 0, \tag{2.7}$$

and from the first moment we get the Euler equation,

$$\partial_\tau \boldsymbol{v} + \mathcal{H}\boldsymbol{v} + (\boldsymbol{v}\cdot\nabla)\,\boldsymbol{v} = -\nabla\Phi - \frac{1}{\rho}\partial_j(\rho\sigma_{ij}). \tag{2.8}$$

From these equations we want to find the equations of motion for the density contrast and the peculiar velocity. With just these two equations we can not get rid of the stress-energy tensor σ_{ij}, but if we take the third moment of the Vlasov equation, we would have to introduce another variable. Because for every higher moment we need to introduce such a new variable, this is a never-ending story. We could find a way out of this by postulating a relation between the stress-energy tensor and the velocities, *e.g.*

$$\sigma_{ij} = -p\delta_{ij} + \eta\left(\partial_i v_j + \partial_j v_i - \frac{2}{3}\delta_{ij}\partial_k v_k\right) + \zeta\delta_{ij}\partial_k v_k \tag{2.9}$$

from standard fluid dynamics with p the pressure and η and ζ viscosity coefficients. In the definition in equation (2.6) one can see that for a single coherent flow $\sigma_{ij} = 0$. On the large scales we are today still in the early stages of gravitational collapse and we can therefore assume we have no multi-streaming on these scales. This makes $\sigma_{ij} \approx 0$ and thus we neglect it in the rest of this chapter. Hence in this approximation, the system of an infinite number of coupled equations reduces just to only two.

Every vector field can be uniquely determined by its divergence and its vorticity.

Before combining these equations, we Fourier transform them. The continuity and Euler equation transform to,

$$\partial_\tau \delta(\boldsymbol{k},\tau) + \theta(\boldsymbol{k},\tau) = S_\alpha, \tag{2.10}$$

$$\partial_\tau \theta(\boldsymbol{k},\tau) + \mathcal{H}(\tau)\theta(\boldsymbol{k},\tau) + \frac{3}{2}\Omega_m\mathcal{H}^2(\tau)\delta(\boldsymbol{k},\tau) = S_\beta, \tag{2.11}$$

where we have defined the velocity divergence, $\theta = \nabla\cdot\boldsymbol{v}$, and

$$S_\alpha = -\int_{\boldsymbol{q}} \alpha(\boldsymbol{q},\boldsymbol{k}-\boldsymbol{q})\theta(\boldsymbol{q},\tau)\delta(\boldsymbol{k}-\boldsymbol{q},\tau)$$

$$S_\beta = -\int_{\boldsymbol{q}} \beta(\boldsymbol{q},\boldsymbol{k}-\boldsymbol{q})\theta(\boldsymbol{q},\tau)\theta(\boldsymbol{k}-\boldsymbol{q},\tau)$$

with

$$\alpha(\boldsymbol{q},\boldsymbol{k}) = \frac{(\boldsymbol{k}+\boldsymbol{q})\cdot\boldsymbol{k}}{k^2}, \qquad \beta(\boldsymbol{q},\boldsymbol{k}) = \frac{(\boldsymbol{k}+\boldsymbol{q})^2(\boldsymbol{k}\cdot\boldsymbol{q})}{k^2} \tag{2.12}$$

We can combine equations (2.10) and (2.11) to get the equation of motion for the density contrast,

$$\partial_\tau^2\delta(\boldsymbol{k},\tau) + \mathcal{H}\partial_\tau\delta(\boldsymbol{k},\tau) - \frac{3}{2}\Omega_m\mathcal{H}^2\delta(\boldsymbol{k},\tau) = (\mathcal{H}+\partial_\tau)S_\alpha - S_\beta \tag{2.13}$$

2.2 Standard Perturbation Theory

Because the density contrast is very small ($\sim 10^{-5}$) on large scales we can treat it perturbatively. First, we try to solve the linear form of equation (2.13) and rewrite the conformal time derivatives to derivatives with respect to the scale factor,

$$\Box\delta_{\rm lin}(\boldsymbol{k},\tau) \equiv a^2\mathcal{H}^2\partial_a^2\delta_{\rm lin}(\boldsymbol{k},a) + a\left(2\mathcal{H}^2 + a\mathcal{H}\partial_a\mathcal{H}\right)\partial_a\delta_{\rm lin}(\boldsymbol{k},a) - \frac{3}{2}\Omega_m\mathcal{H}^2\delta_{\rm lin}(\boldsymbol{k},a) = 0. \tag{2.14}$$

Now we can factorize the solutions,

$$\delta_{\rm lin}(\boldsymbol{k},a) = \delta_{\rm lin}(\boldsymbol{k})D_1(a) \tag{2.15}$$

and solve equation (2.14) for the growth factor $D_1(a)$. This results in a hypergeometric function. We can plug this linear term in the right hand side of the original equations of motion, equation (2.13), and find the second order growth factor, $D_2(a)$. For energy densities $\Omega_m \approx 0.3$ and $\Omega_\Lambda \approx 0.7$, this is very well approximated by $D_2(a) \approx D_1(a)^2$[2].

For a flat Universe without cosmological constant consisting only of non-relativistic matter these equations simplify. In this Einstein-de Sitter (EdS) Universe, where $\Omega_m = 1$ and $\mathcal{H} \sim a^{-1/2}$,

$$D_1^+(a) = a, \qquad \text{and } D_1^- = a^{-3/2} \tag{2.16}$$

are the two independent solutions. The latter is decreasing for increasing scale factor and thus becomes less significant over time. Therefore, we will only use the former, and expand the density contrast as

$$\delta(\boldsymbol{k},a) = \sum_{n=1}^{\infty}\delta^{(n)}(\boldsymbol{k},a) = \sum_{n=1}^{\infty}\delta_{\boldsymbol{k}}^{(n)}a^n, \tag{2.17}$$

and likewise for the velocity divergence,

$$\theta(\boldsymbol{k},a) = \sum_{n=1}^{\infty}\theta^{(n)}(\boldsymbol{k},a) = \sum_{n=1}^{\infty}\theta_{\boldsymbol{k}}^{(n)}a^n. \tag{2.18}$$

Using this expansion in equation (2.13) we find expressions for $\delta_{\boldsymbol{k}}^{(n)}$ up to any order n,

$$\delta_{\boldsymbol{k}}^{(n)} = \int_{\boldsymbol{k}_1,\boldsymbol{k}_2,\ldots,\boldsymbol{k}_n}\delta_D\left(\boldsymbol{k} - \sum_i \boldsymbol{k}_i\right)F_n(\boldsymbol{k}_1,\boldsymbol{k}_2,\ldots,\boldsymbol{k}_n)\delta_{\boldsymbol{k}_1}^{(1)}\delta^{(1)}\boldsymbol{k}_2\ldots\delta_{\boldsymbol{k}_n}^{(1)}, \tag{2.19}$$

$$\theta_{\boldsymbol{k}}^{(n)} = -\mathcal{H}\int_{\boldsymbol{k}_1,\boldsymbol{k}_2,\ldots,\boldsymbol{k}_n}\delta_D\left(\boldsymbol{k} - \sum_i \boldsymbol{k}_i\right)G_n(\boldsymbol{k}_1,\boldsymbol{k}_2,\ldots,\boldsymbol{k}_n)\delta_{\boldsymbol{k}_1}^{(1)}\delta_{\boldsymbol{k}_2}^{(1)}\ldots\delta_{\boldsymbol{k}_n}^{(1)}, \tag{2.20}$$

where we can find the kernels F_n and G_n recursively.

2.3 Power Spectrum

When we say the density of the Universe is homogeneous on large scales, we mean it is statistically homogeneous. Thus, if we take some large enough volume at a random point in space and we take some other random volume of the same size, we expect the mean density to be the same. It also means that all joint multipole probability densities are translation invariant, *i.e.*

$$\langle\delta(\boldsymbol{x}_1)\delta(\boldsymbol{x}_2)\cdots\delta(\boldsymbol{x}_n)\rangle = \langle\delta(\boldsymbol{x}_1+\boldsymbol{x})\delta(\boldsymbol{x}_2+\boldsymbol{x})\cdots\delta(\boldsymbol{x}_n+\boldsymbol{x})\rangle\,.$$

In the case of the two-point correlation function, it means it only depends on $\boldsymbol{x}_1 - \boldsymbol{x}_2$. Because we also assume that the Universe is statistically isotropic, it can not depend on the

angle and therefore the two point correlator only depends on the distance between the two points,

$$\xi(\boldsymbol{x}', \boldsymbol{x}' + \boldsymbol{x}) \equiv \langle \delta(\boldsymbol{x}')\delta(\boldsymbol{x}' + \boldsymbol{x})\rangle = \xi(x). \tag{2.21}$$

A three point function could be described by the size and shape of a triangle.

The power spectrum is defined by the correlation function of the Fourier transformed density fluctuations,

$$\begin{aligned}\left\langle \delta(\boldsymbol{k})\delta(\boldsymbol{k}')\right\rangle &= \int_{\boldsymbol{x}}\int_{\boldsymbol{x}'} \langle \delta(\boldsymbol{x}')\delta(\boldsymbol{x}' + \boldsymbol{x})\rangle \, \mathrm{e}^{-\mathrm{i}\boldsymbol{x}'\cdot\boldsymbol{k}'}\mathrm{e}^{-\mathrm{i}(\boldsymbol{x}'+\boldsymbol{x})\cdot\boldsymbol{k}} && (2.22)\\ &= \delta_D(\boldsymbol{k} + \boldsymbol{k}') \int_{\boldsymbol{x}} \xi(x)\mathrm{e}^{-\mathrm{i}\boldsymbol{x}\cdot\boldsymbol{k}} && (2.23)\\ &\equiv \delta_D(\boldsymbol{k} + \boldsymbol{k}')P(k). && (2.24)\end{aligned}$$

This quantity is also only dependent on the norm of $\boldsymbol{k}$, not on the angle. The bispectrum, the three-point correlation function, would also depend on the angles between the different wave vectors.

If we assume that all joint distributions are Gaussian distributed, Wick's theorem applies,

$$\langle \delta(\boldsymbol{k}_1)\delta(\boldsymbol{k}_2)\cdots\delta(\boldsymbol{k}_n)\rangle = \begin{cases} \sum\limits_{\substack{\text{all pair}\\ \text{associations}}} \prod\limits_{\text{all pairs } (i,j)} \langle \delta(\boldsymbol{k}_i)\delta(\boldsymbol{k}_j)\rangle & \text{if } n \text{ is even} \\ 0 & \text{if } n \text{ is odd} \end{cases} \tag{2.25}$$

Thus for Gaussian initial conditions all correlation functions can be expressed in terms of the power spectrum.

In perturbation theory, we can write

$$\left\langle \delta(\boldsymbol{k})\delta(\boldsymbol{k}')\right\rangle = \left\langle \delta^{(1)}(\boldsymbol{k})\delta^{(1)}(\boldsymbol{k}')\right\rangle + 2\left\langle \delta^{(1)}(\boldsymbol{k})\delta^{(3)}(\boldsymbol{k}')\right\rangle + \left\langle \delta^{(2)}(\boldsymbol{k})\delta^{(2)}(\boldsymbol{k}')\right\rangle + \ldots \tag{2.26}$$

$$P(k) = P_\delta + P_{13} + P_{22} + \ldots \tag{2.27}$$

if the linear density perturbations are Gaussian. Without the condition of Gaussianity, there would also be terms as P_{12}, a term dependent on the bispectrum. Therefore non-Gaussianity arises when the initial bispectrum does not vanish.

2.3.1 Initial Power Spectrum

Eventually we want to say something about the very young Universe. Therefore we have to know how primordial perturbations evolve through time such that we can relate the measurements now to the situation there must have been.

We expect that the earliest fluctuations are formed before the end of inflation. The mechanisms causing these fluctuations are unknown, but are thought to be very short wavelength, even smaller than the Planck length. The wavelength of these fluctuations keep growing with the scale factor a. The Hubble radius during inflation is however constant, so (almost all) perturbation modes are larger than the horizon at the end of inflation, $k\tau \ll 1$. After inflation follows the radiation epoch, where the Hubble radius grows as a^2, such that more and more larger modes enter the Hubble radius.

When outside the horizon perturbation modes *freeze out*, they do not evolve apart from spreading out due to the growing scale factor. During radiation era, the pressure is too large for structures to form. Therefore, modes entering the horizon well before matter-radiation equality only oscillate while their amplitudes stay the same. The modes entering the horizon long past matter-radiation equality immediately start to grow.

Of course the power spectrum today depends on the primordial power spectrum. The spectrum for large scales today, consisting of the modes entered in the matter-dominated era, has the same k-dependence as the primordial power spectrum. The modes that entered in the radiation-dominated era, were suppressed till the time of matter-radiation equality. Therefore we see a peak in the power spectrum in figure 2.3.

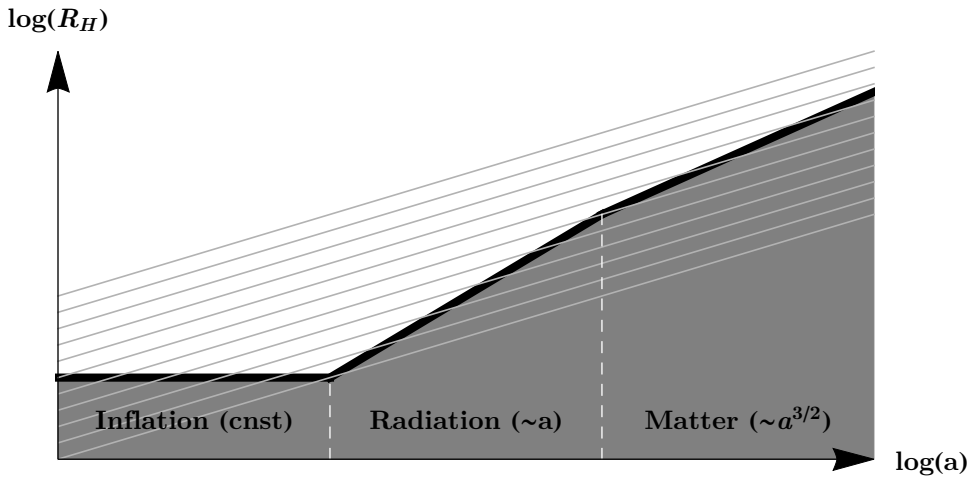

Figure 2.2: Matter perturbation modes (thin grey lines) leave the horizon during inflation when the horizon is constant. They enter at different times in the radiation dominated era or the subsequent matter era.

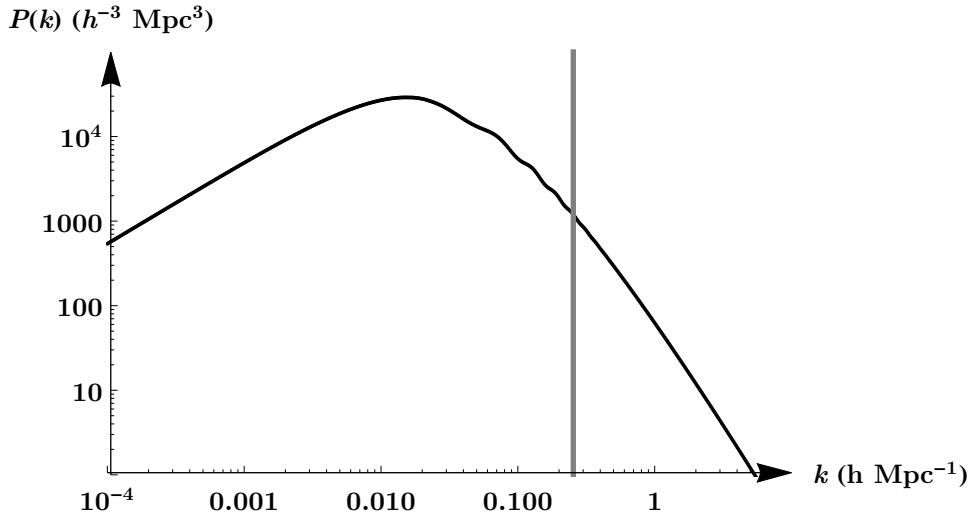

Figure 2.3: The power spectrum according to WMAP. The grey vertical line is at $k_{\mathrm{NL}}(\approx 0.2)$ so left of that line everything is still evolving linearly.

2.4 Self-Similarity

In an Einstein-de Sitter Universe there is no preferred scale, and therefore the equations of motion should allow self-similar solutions. This means that a scaling of the fields together with a scaling of the space and time coordinates should result in another solution. If the fields are known at a given time, then the total evolution of the fields is known.

We can find self-similar solutions by introducing the scaling,

$$\tilde{\delta}(\boldsymbol{x}, \tau) = \lambda_\delta \delta(\lambda_x \boldsymbol{x}, \lambda_\tau \tau) \tag{2.28}$$

and similar for $\boldsymbol{v}$ and Φ, and plug this in equations (2.7) and (2.8). Then we get the the scalings,

$$\tilde{\delta}(\boldsymbol{x}, \tau) = \delta(\lambda_x \boldsymbol{x}, \lambda_\tau \tau) \tag{2.29a}$$

$$\tilde{\boldsymbol{v}}(\boldsymbol{x}, \tau) = \frac{\lambda_\tau}{\lambda_x} \boldsymbol{v}(\lambda_x \boldsymbol{x}, \lambda_\tau \tau) \tag{2.29b}$$

$$\tilde{\Phi}(\boldsymbol{x},\tau) = \left(\frac{\lambda_\tau}{\lambda_x}\right)^2 \Phi(\lambda_x \boldsymbol{x}, \lambda_\tau \tau) \tag{2.29c}$$

$$\tilde{\sigma}_{ij}(\boldsymbol{x},\tau) = \left(\frac{\lambda_\tau}{\lambda_x}\right)^2 \sigma_{ij}(\lambda_x \boldsymbol{x}, \lambda_\tau \tau). \tag{2.29d}$$

This does not work in ΛCDM, because there we do not have $\mathcal{H} \propto \tau^{-1}$.

Though for every choice of λ_τ and λ_x the scalings in equation (2.29) give solutions of the equations of motion, they are not part of the same cosmology for arbitrary choices. If we want to find a family of solutions to be part a sample of the same initial conditions, we have to demand that the power spectrum is the same for all members of the family.

Therefore, we require

$$\tilde{\Delta}(k,\tau) = \Delta(\lambda_x^{-1} k, \lambda_\tau \tau). \tag{2.30}$$

We will first look at very early times, when the linear theory still holds. If we assume power law initial conditions with index n, *i.e.* $\Delta_{\text{in}}(k,\tau) \propto k^{3+n}\tau^4$, the initial power spectrum scales as

$$\tilde{\Delta}_{\text{in}}(k,\tau) = \lambda_x^{-3-n} \lambda_\tau^4 \Delta_{\text{in}}(k,\tau). \tag{2.31}$$

If we make the choice,

$$\lambda \equiv \lambda_\tau = \lambda_x^{\frac{3+n}{4}}, \tag{2.32}$$

then the power spectra are the same, and thus the picked solutions of the equations of motion are just other samples of the same initial power spectrum. Because the power spectrum is an ensemble averaged quantity, it should be equal for all times and all choices of λ,

$$\Delta(k,\tau) = \tilde{\Delta}(k,\tau) = \Delta(\lambda^{-\frac{4}{3+n}} k, \lambda\tau) \tag{2.33}$$

which means the power spectrum can only depend on wave number and time in the combination $k\tau^{\frac{4}{3+n}}$. Thus we write,

$$\Delta(k,\tau) = \Delta(k/k_{\text{NL}}), \tag{2.34}$$

with

$$k_{\text{NL}} \equiv \frac{2\pi^2}{Aa^2} \propto \tau^{-4}. \tag{2.35}$$

First we said that there is no preferred scale for the equations of motion. Now we see that if we demand the self-similar solution to be part of the same cosmology there arises a scale, k_{NL}. Hence, we conclude that there is only one typical scale in a cosmology and that is the non-linear scale. Furthermore, we should be able to express all solutions in terms of this scale only.

Chapter 3

Effective Field Theory

For scales where the density contrast is much smaller than unity, perturbation theory gives a very good description. On smaller scales however, the contrast becomes non-linear and the perturbative expansion diverge. The easiest thing to do is to find the scale where it becomes non-linear and cut it off from there, but if you follow this procedure your theory becomes cut-off dependent and thus unphysical.

Small scale modes can give a backreaction on long scale modes and should be included. In Effective Field Theory we add terms to the equation of motion to describe the influence of the short scale on the long scale perturbations. Comparable to a regular fluid, where we do not need to know all the interactions on molecular level to give a macroscopic description, but knowing parameters like the density and the viscosity suffices.

3.1 Integrating out short wavelengths

If we include all wavelengths, the perturbative expansion starts to diverge for short wavelengths. We want to smooth the density perturbations such that these divergences disappear. Here we choose the Gaussian smoothing function,

$$W_\Lambda(\boldsymbol{x}) = \left(\frac{\Lambda}{\sqrt{2\pi}}\right)^3 \mathrm{e}^{-\frac{1}{2}\Lambda^2 x^2}, \tag{3.1}$$

and define the smoothed quantities as the convolution with this function,

$$[\mathcal{O}]_\Lambda(\boldsymbol{x},\tau) = \int \mathrm{d}^3x'\, W_\Lambda(\boldsymbol{x}-\boldsymbol{x}')\mathcal{O}(\boldsymbol{x}').$$

This will smooth all fluctuations with wavelengths smaller than $1/\Lambda$, as is shown in figure 3.1.

Using this method, we want to smooth the fluid equations for a pressureless fluid, *i.e.* equations (2.7) and (2.8) with $\sigma_{ij} = 0$. We start with defining the smoothed quantities,

$$\rho_\ell(\boldsymbol{x}) \equiv [\rho]_\Lambda(\boldsymbol{x}) = \int_{\boldsymbol{x}'} W_\Lambda(\boldsymbol{x}-\boldsymbol{x}')\rho(\boldsymbol{x}'), \tag{3.2}$$

$$\phi_\ell(\boldsymbol{x}) \equiv [\phi]_\Lambda(\boldsymbol{x}) = \int_{\boldsymbol{x}'} W_\Lambda(\boldsymbol{x}-\boldsymbol{x}')\phi(\boldsymbol{x}'), \tag{3.3}$$

$$\rho_\ell \boldsymbol{v}_\ell(\boldsymbol{x}) \equiv [\rho\boldsymbol{v}]_\Lambda(\boldsymbol{x}) = \int_{\boldsymbol{x}'} W_\Lambda(\boldsymbol{x}-\boldsymbol{x}')\rho(\boldsymbol{x}')\boldsymbol{v}(\boldsymbol{x}'). \tag{3.4}$$

One should note that this means $\boldsymbol{v}_\ell \neq [\boldsymbol{v}]_\Lambda$.

If we apply this smoothing on our equations of motion, we get the smoothed continuity and Euler equations (see appendix A.1 for the derivation), respectively,

$$\delta_\tau \rho_\ell + 3\mathcal{H}\rho_\ell + \partial_i(\rho_\ell v_\ell^i) = 0, \tag{3.5}$$

$$\partial_\tau v_\ell^i(\boldsymbol{x},\tau) + \mathcal{H}v_\ell^i(\boldsymbol{x},\tau) + v_\ell^j(\boldsymbol{x},\tau)\partial_j v_\ell^i(\boldsymbol{x},\tau) = -\frac{1}{\rho_\ell}\partial_j\left[\tau^{ij}\right]_\Lambda, \tag{3.6}$$

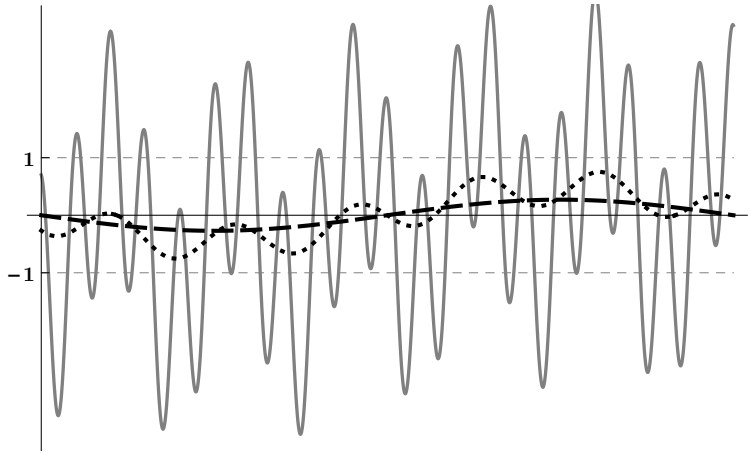

Figure 3.1: A signal consisting of long and short wavelength modes (grey, solid), and smoothed with a large (dashed) and small (dotted) smoothing scale.

where τ^{ij} is the effective stress-energy tensor,

$$\tau^{ij} = \rho v_{\rm s}^i v_{\rm s}^j - \frac{\delta^{ij}\partial_k\phi_{\rm s}\partial_k\phi_{\rm s} - 2\partial_i\phi_{\rm s}\partial_j\phi_{\rm s}}{8\pi G}. \tag{3.7}$$

This stress-energy tensor is manifestly dependent on the short-wavelength modes. However, we will not measure these, possibly very large, small-scale density fluctuations. Because we are only interested in their effects on the large-scale perturbations, we will take expectation values of the stress-energy tensor. The expectation value does not longer depend on the small scale modes, but rather only on the large scale perturbations, such that we can expand it in δ_ℓ using a simple Taylor expansion,

$$\left\langle \left[\tau^{ij}\right]_\Lambda \right\rangle_{\delta_\ell} = \left\langle \left[\tau^{ij}\right]_\Lambda \right\rangle_{\delta_\ell}\Big|_{\delta_\ell=0} + \left.\frac{\partial \left\langle \left[\tau^{ij}\right]_\Lambda \right\rangle_{\delta_\ell}}{\partial\delta_\ell}\right|_{\delta_\ell=0} \delta_\ell + \dots \tag{3.8}$$

We can write this in the most general form up to first order in perturbations which is symmetric,

$$\left\langle \left[\tau^{ij}\right]_\Lambda \right\rangle_{\delta_\ell} = A\delta^{ij} + B\delta^{ij}\delta_\ell + C\delta^{ij}\partial_k v_\ell^k + D\left(\partial_i v_\ell^j + \partial_j v_\ell^i\right). \tag{3.9}$$

We can rewrite this in a trace and a trace-free part in the suggestive form

$$\left\langle \left[\tau^{ij}\right]_\Lambda \right\rangle_{\delta_\ell} = \bar{p}_{\rm eff}\delta^{ij} + \bar{\rho}\left[c_{\rm s}^2\delta_\ell\delta^{ij} - \frac{c_{\rm bv}^2}{\mathcal{H}}\delta^{ij}\partial_k v_\ell^k - \frac{3c_{\rm sv}^2}{4\mathcal{H}}\left(\partial_j v_\ell^i + \partial_i v_\ell^j - \frac{2}{3}\delta^{ij}\partial_k v_\ell^k\right)\right] + \Delta\tau^{ij} + \dots \tag{3.10}$$

which is the stress-energy tensor of an imperfect fluid, with $p_{\rm eff}$ the effective pressure, $c_{\rm s}$ the speed of sound, and $c_{\rm bv}$ and $c_{\rm sv}$ the bulk and shear viscosity, respectively.

3.2 Effective Field Theory Parameters

Now we have an expression for the effective stress-energy tensor in equation (3.10), we want to know what the parameters in this expression are. We already know they should provide counterterms for the UV-divergences in the perturbative expansion of the power spectrum, but in this section we want to show it explicitly.

First look at the trace of the effective stress-energy tensor,

$$\langle [\tau]_\Lambda \rangle \equiv \left\langle \left[\delta_{ij}\tau^{ij}\right]_\Lambda \right\rangle = 3\bar{p}_{\rm eff} + 3\bar{\rho}c_{\rm s}^2\delta_\ell - 3c_{\rm bv}^2\frac{\theta_\ell}{\mathcal{H}} \tag{3.11}$$

We assume the long-wavelength perturbations to be Gaussian and we know from equation (2.20) $\theta_\ell = \theta^{(1)} = -\mathcal{H}\delta_\ell$. Hence,

$$\bar{p}_{\text{eff}} = \frac{1}{3}\lim_{k\to 0}\langle\tau\rangle \qquad \text{and} \qquad c_{\text{s}}^2 + c_{\text{bv}}^2 = \frac{1}{\bar{\rho}}\frac{\langle\delta_\ell p_{\text{eff}}\rangle}{\langle\delta_\ell\delta_\ell\rangle}. \tag{3.12}$$

If we now look at the traceless part,

$$\left\langle\left[\hat{\tau}^{ij}\right]_\Lambda\right\rangle \equiv \left\langle\left[\tau^{ij} - \frac{1}{3}\delta^{ij}\tau\right]_\Lambda\right\rangle = -\frac{3c_{\text{sv}}^2}{4\mathcal{H}}\left(\partial_j v_\ell^i + \partial_i v_\ell^j - \frac{2}{3}\delta^{ij}\partial_k v_\ell^k\right), \tag{3.13}$$

we can subsequently define,

$$\sigma_{\text{eff}} = \frac{1}{\bar{\rho}}\frac{\partial_i\partial_j}{\partial^2}\left\langle\left[\hat{\tau}^{ij}\right]_\Lambda\right\rangle = -c_{\text{sv}}^2\frac{\theta_\ell}{\mathcal{H}} = c_{\text{sv}}^2\delta_\ell \tag{3.14}$$

and using correlators over long wavelength perturbations again,

$$c_{\text{sv}}^2 = \frac{\langle\delta_\ell\sigma_{\text{eff}}\rangle}{\langle\delta_\ell\delta_\ell\rangle}. \tag{3.15}$$

Using equations (3.12) and (3.15) with the stress-energy tensor as in equation (3.7), we find (the derivation can be found in appendix A.2)

$$c_{\text{comb}}^2 = c_{\text{s}}^2 + c_{\text{bv}}^2 + c_{\text{sv}}^2 = \frac{61}{70}\frac{1}{2\pi^2}\mathcal{H}^2\int \mathrm{d}q\, P_\delta(q). \tag{3.16}$$

With adding the effective terms to the equations of motion, the expansion of the density contrast becomes,

$$\delta = \delta_1 + \delta_2 + \delta_3 + \ldots + \delta_{c_{\text{s}}^2} + \ldots$$

and the expansion of the power spectrum, *cf.* equation (2.27),

$$P = P_\delta + P_{13} + P_{22} + P_{c_{\text{s}}^2} + \ldots. \tag{3.17}$$

To start with computing $\delta_{c_{\text{s}}^2}$, we define the Green's function,

$$\Box G(a,\tilde{a}) = \delta_D(a-\tilde{a}), \tag{3.18}$$

with $\Box$ the operator defined in equation (2.14). In the effective theory we have the equations of motion[3],

$$\Box\delta_\ell = (c_{\text{s}}^2 + c_{\text{bv}}^2)\partial^2\delta_\ell + c_{\text{sv}}^2 a\partial^2\partial_a\delta_\ell, \tag{3.19}$$

such that if we write $\delta_\ell = \delta_{\text{lin}} + \delta_{c_{\text{s}}^2}$ we get,

$$\delta_{c_{\text{s}}^2}(\boldsymbol{k},a) = \int \mathrm{d}\tilde{a}\, G(a,\tilde{a})k^2\left[c_{\text{s}}^2 + c_{\text{bv}}^2 + c_{\text{vis}}^2\tilde{a}\partial_{\tilde{a}}\right]\delta_\ell(\boldsymbol{k},\tilde{a}) \tag{3.20}$$

In EdS the Green's function takes the form,

$$G(a,\tilde{a}) = \theta_H(a-\tilde{a})\frac{2}{5\mathcal{H}_0^2}\left[\left(\frac{\tilde{a}}{a}\right)^{3/2} - \frac{a}{\tilde{a}}\right], \tag{3.21}$$

where θ_H is the Heaviside function. Plugging this in equation (3.20), results in

$$\delta_{c_{\text{s}}^2} = -\frac{a}{9\mathcal{H}_0^2}k^2 c_{\text{comb}}^2\delta_\ell. \tag{3.22}$$

With this result we can compute $P_{c_s^2}$ by taking expectation values,

$$\langle \delta^{(1)}_{\boldsymbol{k}} \delta_{c_s^2(\boldsymbol{p})} \rangle = -\frac{a}{9\mathcal{H}_0^2} p^2 c^2_{\text{comb}} \langle \delta^{(1)}_{\boldsymbol{k}} \delta^{(1)}_{\boldsymbol{p}} \rangle \tag{3.23}$$

$$= -\frac{61a}{630\pi^2} \frac{\mathcal{H}^2}{\mathcal{H}_0^2} p^2 \delta_D(\boldsymbol{k}+\boldsymbol{p}) P_\delta(k) \int \mathrm{d}q\, P_\delta(q), \tag{3.24}$$

$$P_{c_s^2}(k) = -\frac{61}{630\pi^2} k^2 P_\delta(k) \int \mathrm{d}q\, P_\delta(q) \tag{3.25}$$

If we take the primordial power spectrum to follow a power law with spectral index n, *i.e.* $P_\delta(k) = Ak^n$, then for $n \geq 0$ we find,

$$P_{c_s^2}(k) = -\frac{1}{(2\pi)^3} \frac{244}{315} \pi A^2 k^{2+n} \int_0^{k_c} \mathrm{d}q\, q^n = -\frac{1}{(2\pi)^3} \frac{244}{315(n+1)} \pi A^2 k^{2+n} k_c^{n+1}\,. \tag{3.26}$$

We claimed that the effective terms would cancel the short wavelength (UV) divergences that arise in SPT. If we compare equation (3.26) with equation (A.70), we see that it indeed does.

3.3 Self-Similarity in EFT

In section 2.4 we have shown that there are self-similar solutions of the equations of motion in an Einstein-de Sitter Universe. This self-similarity should of course be maintained in the effective theory. If we take the same scaling as in equation (2.29), and plug it in the smoothed Euler equation, equation (3.6), we find the scaling

$$\left[\tilde{\tau}^{ij}\right]_\Lambda (\boldsymbol{x}, \tau) = \left(\frac{\lambda_\tau}{\lambda_x}\right)^2 \left[\tau^{ij}\right]_\Lambda (\lambda_x \boldsymbol{x}, \lambda_\tau \tau). \tag{3.27}$$

If we compare this with equation (3.10), we conclude that effective parameters scale as

$$c_{\text{s}}^2, c_{\text{bv}}^2, c_{\text{sv}}^2 \propto \left(\frac{\lambda_x}{\lambda_\tau}\right)^2. \tag{3.28}$$

These parameters represent averages over short modes and thus the scaling should only be satisfied if it conserves the initial power spectrum. Using equation (2.32), we find the time dependence of the coefficients of the effective theory,

$$c_{\text{s}}^2, c_{\text{bv}}^2, c_{\text{sv}}^2 \propto \tau^{\frac{2-2n}{3+n}}. \tag{3.29}$$

Chapter 4

The Spherical Collapse Model

Until now we looked at general fluctuations in matter density and had to resort to perturbative methods (in SPT) or simulations (in EFT). Many physical problems which are hard to resolve for general conditions become if we simplify significantly if we put enough constraints on it. Although those constraints are not entirely realistic, the derived analytic results may give a good insight in the physics involved and can serve as a first order approximation for real life circumstances. Remember for instance the parabolic trajectory of thrown basketballs when friction is neglected, a situation which can be found in every high school physics text book.

4.1 Newtonian Spherical Collapse

When studying large scale structures we look at the evolution of density distribution functions in three dimensions. To simplify this, we will constrain the distribution function to be spherically symmetric at initial time – and by that for all times.

We start with the Newtonian equation

$$\ddot{R} \equiv \frac{\mathrm{d}^2 R}{\mathrm{d}t^2} = -\frac{GM}{R^2} \tag{4.1}$$

where R is radius of a mass shell and M is the mass enclosed by that radius.

We can write this as

$$\frac{\mathrm{d}}{\mathrm{d}t}\left(\frac{\mathrm{d}R}{\mathrm{d}t}\right)^2 = 2\frac{\mathrm{d}}{\mathrm{d}t}\left(\frac{GM}{R}\right), \tag{4.2}$$

which results in,

$$\dot{R}^2 - \frac{2GM}{R} = F, \tag{4.3}$$

where F is some integration constant (independent of t). This equation can be solved by the parametrization

$$R(\eta) = \frac{GM}{|F|}(1-\cos(\eta)), \qquad t(\eta) = \frac{GM}{|F|^{3/2}}(\eta - \sin(\eta)) + t_0, \tag{4.4}$$

for $F < 0$, and by

$$R(\eta) = \frac{GM}{|F|}(\cosh(\eta)-1), \qquad t(\eta) = \frac{GM}{|F|^{3/2}}(\sinh(\eta) - \eta) + t_0, \tag{4.5}$$

in the case $F > 0$. In the former case the radius is first expanding, and later shrinking, this corresponds to a matter collapse and thus an initial overdensity. The latter parametrization is of a exponentially increasing radius and therefore corresponds to an initial underdensity.

The integration constant F only depends on the initial density distribution within R, as long as the energy outside is distributed spherically symmetric. This means that the collapse is independent of the (initial) density distribution outside the sphere we are looking at in this Newtonian picture. In this thesis we will only consider spherically symmetric initial overdensities, so we only consider equation (4.4). Aside from the sign, the value of F does not seem to make much sense physically. Therefore we define some initial time $t_{\rm in} \equiv t(\eta_{\rm in})$ and initial radius $R_{\rm in} \equiv R(\eta_{\rm in})$ with $\eta_{\rm in} \ll 1$, and write

$$R(\eta) = R_{\rm in}\frac{1-\cos\eta}{1-\cos\eta_{\rm in}}, \qquad t(\eta) = t_{\rm in}\frac{\eta-\sin\eta}{\eta_{\rm in}-\sin\eta_{\rm in}} \tag{4.6}$$

In an EdS universe, $H = \frac{2}{3t}$, and thus from the Friedman equation the background matter density is,

$$\bar{\rho} = \frac{1}{6\pi G_{\rm N} t^2}. \tag{4.7}$$

We will look at a *top hat* density distribution, *i.e.* a sphere with uniform density,

$$\rho = \frac{3M}{4\pi R^3} \tag{4.8}$$

Combining these we can give an expression for the density contrast in spherical collapse,

$$1+\delta = \frac{\rho}{\bar{\rho}} = \frac{9G_{\rm N}Mt^2}{2R^3}, \tag{4.9}$$

or in terms of the earlier defined initial conditions,

$$1+\delta = (1+\delta_{\rm in})\left(\frac{t}{t_{\rm in}}\right)^2\left(\frac{R_{\rm in}}{R}\right)^3. \tag{4.10}$$

If we plug the parametric equations of equation (4.6) in equation (4.1) and fill in the initial conditions, we get the relation between the initial conditions

$$\frac{(\eta_{\rm in}-\sin\eta_{\rm in})^2}{(1-\cos\eta_{\rm in})^3} = -\frac{GMt_{\rm in}^2}{R_{\rm in}^3}. \tag{4.11}$$

Using this in equation (4.9), results in the simple parametric expression

$$1+\delta = \frac{9}{2}\frac{(\eta-\sin\eta)^2}{(1-\cos\eta)^3} \tag{4.12}$$

4.2 Spherically Symmetric Equations of Motion

We go back to the equations of motions derived from the Vlasov equation in section 2.1. In the case of spherical symmetry, the density contrast only depends on the distance to the point of symmetry and the time. This gives us the continuity and Euler equation, respectively, for spherical collapse, *cf.* equations (2.7) and (2.8),

$$\partial_\tau\delta + v\partial_r\delta + (1+\delta)\theta = 0 \tag{4.13}$$

$$\partial_\tau\theta + \mathcal{H}\theta + \theta\partial_r v + v\partial_r^2 v + \partial_r\Phi = 0 \tag{4.14}$$

where $\boldsymbol{v} = (v_r, v_\theta, v_\phi) = (v, 0, 0)$, r is the distance to the point of symmetry and $\theta \equiv \nabla\cdot\boldsymbol{v} = r^{-2}\partial_r(r^2 v)$. We still have have the Poisson equation, equation (2.2), which means under these conditions $\partial_r^2\Phi = -\frac{3}{2}\mathcal{H}^2\delta$. We can transform these equations into the Lagrangian equations

$$D_\tau\delta + (1+\delta)\theta = 0 \tag{4.15}$$

$$D_\tau\theta + \mathcal{H}\theta + \frac{1}{3}\theta^2 + \frac{3}{2}\mathcal{H}^2\delta = 0, \tag{4.16}$$

where $D_\tau = \partial_\tau + v\partial_r$ is the convective derivative with respect to conformal time. Convective derivatives[1] are derivatives for fixed Lagrangian coordinates.

We can combine those to get the equation of motion for the density,

$$D_\tau^2\delta + \mathcal{H}D_\tau\delta - \frac{3}{2}\mathcal{H}^2\delta = \frac{4}{3}\frac{(D_\tau\delta)^2}{1+\delta} + \frac{3}{2}\mathcal{H}^2\delta^2 \tag{4.17}$$

$$\ddot{\delta} + 2H\dot{\delta} - \frac{3}{2}H^2\delta = \frac{4}{3}\frac{\dot{\delta}^2}{1+\delta} + \frac{3}{2}H^2\delta^2. \tag{4.18}$$

where the dots denote convective derivatives with respect to regular time, $D_t = \partial_t + a^{-1}v\partial_r$.

If we use the identifications

$$M \equiv \frac{4\pi}{3}R^3\bar{\rho}(1+\delta), \qquad H^2 = \frac{8\pi G_\mathrm{N}}{3}\bar{\rho}, \tag{4.19}$$

equation (4.18) and equation (4.1) are equivalent. Notice that we did not use a top hat assumption here. Therefore we can conclude that the Lagrangian equations of motion for a general spherically symmetric density contrast are the same as the Eulerian equations for a top hat distribution. This should not come as a surprise, because the density is the same everywhere in a top hat distribution and therefore it does not matter whether you move along with a particle or stay at a fixed position, as long as it is within the overdense region at least.

Notice also that in the Lagrangian formalism the density ρ is the mean density of the overdense region and thus the exact distribution is not important – as long as it is spherically symmetric of course. This is a familiar result, because gravity outside a spherically symmetric object does never depend on the density distribution rather than on the total mass.

4.3 Perturbation Theory in Spherical Collapse

In most generic cases of structure formation the perturbative expansion does not converge to the real solution for arbitrary large density contrasts. In this section we will show that in spherical collapse it does converge for any value of δ. However, for spherically symmetric underdensities the expansion still diverges.

We have the expression for the density contrast,

$$\delta = \frac{9G_\mathrm{N}Mt^2}{2R^3} - 1 = (1+\delta_\mathrm{in})\frac{(1-\cos\eta_\mathrm{in})^3}{(\eta_\mathrm{in}-\sin\eta_\mathrm{in})^2}\frac{(\eta-\sin\eta)^2}{(1-\cos\eta)^3} - 1, \tag{4.20}$$

in a very suggestive form, where we can see immediately it holds for the initial conditions. We have already seen in equation (4.12) that we can simplify this to

$$\delta = \frac{9}{2}\frac{(\eta-\sin\eta)^2}{(1-\cos\eta)^3} - 1. \tag{4.21}$$

When working in perturbation theory, we want to expand this in terms of the linear term δ_lin. In an Einstein-de Sitter Universe the linear terms go with the scale factor, $\delta_\mathrm{lin} \propto a \propto t^{2/3}$. Hence,

$$\delta_\mathrm{lin} = \frac{3}{5}\left(\frac{3}{4}(\eta-\sin\eta)\right)^{2/3}. \tag{4.22}$$

Expanding the density contrast,

$$\delta = \sum_{n\geq 1}\frac{\nu_n}{n!}\delta_\mathrm{lin}^n - 1,$$

[1] There are many names for this derivative, among others: the material derivative, the Lagrangian derivative, the Stokes derivative, the hydrodynamic derivative.

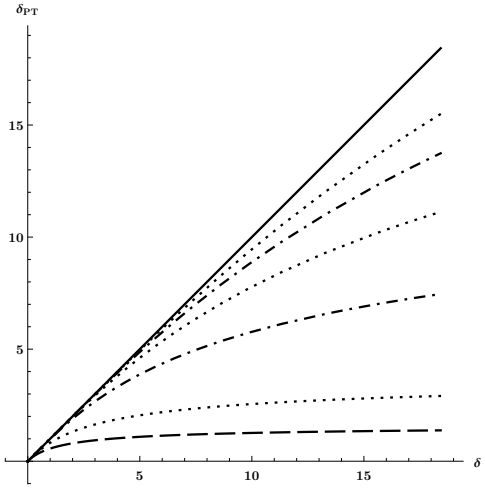

(a) Perturbative expansion of growing initial overdensities

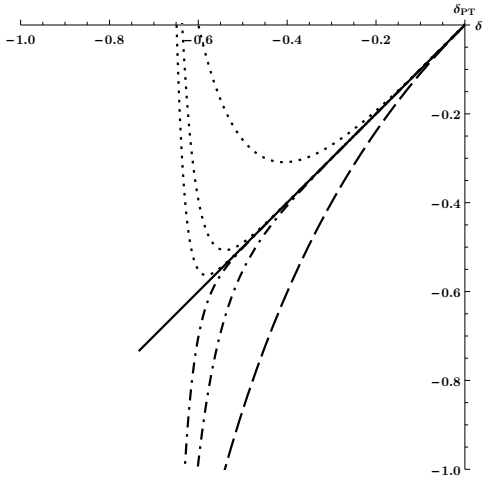

(b) Perturbative expansion of growing initial underdensities

Figure 4.1: The density contrasts found using perturbation theory converge to the real solution in spherical collapse but diverges for underdensities when $\delta \approx -0.7$. The solid black line is the fully non-linear solution, the dashed line is the linear solution, the dotted (dash-dotted) are perturbative expansions up to order 2, 8 and 14 (5 and 11).

and using the expansion of equation (4.21),

$$\delta = -\frac{3}{20}\eta^2 + \frac{13}{1400}\eta^4 - \frac{17}{56000}\eta^6 + \dots, \tag{4.23}$$

to match the expansion coefficients ν_n up to any order, one will find,

$$\nu_1 = 1, \qquad \nu_2 = \frac{34}{21}, \qquad \nu_3 = \frac{682}{189}, \qquad \nu_4 = \frac{446440}{43659}. \tag{4.24}$$

We can see in figure 4.1a that the perturbative expansion converges for all overdensities. This means that in spherical collapse we can always use perturbation theory to find solutions because it does not break down anywhere.

In the case of a spherical underdensity, which results in the growth of a spherical void, we can follow the same procedure as for the overdensity. We start instead with the parametric equations equation (4.5) and find the parametric equation for the density contrast,

$$\delta = \frac{(\sinh\eta - \eta)^2}{(\cosh\eta - 1)^3} - 1 \tag{4.25}$$

and expand this in δ_{lin}. We get exactly the same expansion coefficients as in equation (4.24). Again, we plot the perturbative expansion, see figure 4.1b, and conclude that for underdensities the perturbative expansion does diverge for every order at $\delta \approx -0.7$.

The expansion coefficient ν_n being the same for under and overdensities is not surprising. We can see this if we compute these coefficients directly from section 2.2. For spherically symmetric densities, the angular integrals in equation (2.19) is only over the kernels and result in pure numbers. With the symmetrised kernel,

$$F_2(\boldsymbol{k}_1, \boldsymbol{k}_2) = \frac{5}{7} + \frac{1}{2}\mu\left(\frac{k_1}{k_2} + \frac{k_2}{k_1}\right) + \frac{2}{7}\mu^2, \qquad \mu = \frac{\boldsymbol{k}_1 \cdot \boldsymbol{k}_2}{k_1 k_2}, \tag{4.26}$$

we get the coefficient

$$\nu_2 = \int \frac{\mathrm{d}\Omega_k}{2\pi} F_2(\boldsymbol{k}, \boldsymbol{q}) = \frac{1}{2\pi}\int_0^{2\pi} \mathrm{d}\phi \int_0^{\pi} \mathrm{d}\theta\, \sin\theta F_2 \tag{4.27}$$

$$= \int_0^1 \mathrm{d}\mu\, F_2 = \frac{34}{21}. \tag{4.28}$$

We can do this for all kernels and find all the expansion coefficients. In this derivation we did not assume under or overdensities initially. Therefore this should hold for both cases.

4.4 Effective Parameters in Spherical Collapse

We have derived the equations of motion in the Lagrangian picture and have a parametric expression for R and t. With this we have all the means to derive an (parametric) expression for the effective parameters. Furthermore, we know that the perturbative expansion converges to the real solution, so we can compute the parameters up to any order.

4.5 Self-Similarity in Spherical Collapse

In section 2.4 we have shown that standard perturbation theory allows self-similar solutions in Einstein-de Sitter. Because SPT gives a convergent description of spherical collapse, the spherical collapse solutions should also be self-similar.

If we consider a solution of equation (4.1), given by $R(R_{\rm in}, t)$ there is a family of solutions

$$R'(R_{\rm in}, t) = \lambda R(R_{\rm in}, \lambda^{-3/2} t). \tag{4.29}$$

Plugging in $t = t_{\rm in}$ shows that R' and R have the same initial conditions if and only if $R \propto t^{2/3}$. In that case both solutions are identical, choosing a different scaling gives the same solution at a different time.

This rescaling was for any $M(R_{\rm in})$, independent of the density distribution. For a specific mass profile, we can do the same as in section 2.4. We assume we have a found a solution $R(q, t)$ of equation (4.1) for a density profile $M(q)$, and plug the scaling

$$\tilde{R}(R_{\rm in}, t) \equiv \lambda_R R(\lambda_{R_{\rm in}} R_{\rm in}, \lambda_t t) \tag{4.30}$$

back in. This gives the condition on the density profile,

$$\frac{M(R_{\rm in}/\lambda_{R_{\rm in}})}{M(R_{\rm in})} = \lambda_t^2 \lambda_R^3. \tag{4.31}$$

This condition is only satisfied for all scaling factors if

$$\frac{M(R_{\rm in}/\lambda_{R_{\rm in}})}{M(R_{\rm in})} = \lambda_{R_i}^{\alpha}. \tag{4.32}$$

The initial condition $R(t_{\rm in}) \equiv R_{\rm in}$ requires $\lambda_{R_{\rm in}} = \lambda_R$, and thus, combining above equations,

$$\lambda_t = \lambda_R^{\frac{\alpha-3}{2}}. \tag{4.33}$$

Considering an initial scale invariant power spectrum with index n, requires furthermore, *cf.* equation (2.32)

$$\lambda_t = \lambda_R^{\frac{3(3+n)}{4}}, \tag{4.34}$$

which results in the constraint on α,

$$\alpha = \frac{15 + 3n}{2}. \tag{4.35}$$

Chapter 5

Experiments

The limit on the amount of information that could be extracted from the two-dimensional picture of the CMBR is almost reached. The three-dimensional model of large scale structures is now the most obvious place to look for more clues about the earliest times of our Universe. In the last few chapters we have reviewed the theory of structure formation, in this chapter we will look at the experimental side.

Large scale structures are measured using redshift surveys. In these surveys large parts of the sky are searched for luminous objects. Measuring the angular coordinates is trivial; to find the radial coordinate the spectrum is analysed and the redshift is measured. We will first look at the theory behind the experiments and thereafter review some of the experiments. Will Percival wrote great lecture notes about large scale observations[4], here we will pick out some of the topics discussed in there.

5.1 Theory Behind the Experiments

In redshift surveys the angular position and the redshift of galaxies is measured. Because the Universe expands and we can measure at what rate it is expanding, the recession velocity of an observed galaxy is enough to determine the distance to that galaxy. To determine the recession velocity we can use the redshift: the faster a galaxy is moving away from us, the more its emitted radiation is redshifted.

The observed light profiles can be fitted to templates or training spectra in two different ways. We can either use the broad-band colours or we can use the spectrum. The latter method uses the absorption and emission lines and is therefore much more precise, with typical errors of $0.001(1+z)$ to $0.0001(1+z)$ against $0.05(1+z)$ for the so called photometric redshift measurements. Unfortunately it is not always possible to measure the spectrum from a galaxy, so it is a trade off between the number of data points and the accuracy.

When we have measured many galaxies we want to translate the observed galaxy distribution to the real density contrast. First of all, we have to take into account where we could have measured galaxies. There could be for instance a star in the path between us and a galaxy which prevents us from measuring that galaxy. Furthermore, if our measurements are magnitude-limited, we can only observe the brightest galaxies on long distances. To take all these things into account, we have to use a mask. A mask is what we expect to measure if we assume a random sample of homogeneously distributed galaxies with the expected background density $\bar{\rho}$.

We observe only the galaxies, while we want to measure the matter densities. If we assume that the galaxies form just a Poisson sample of the total matter density, we use that to apply weights to the positions in our mask. This assumption is unfortunately only an approximation.

What we eventually want to measure is the power spectrum averaged over all angles. We can compute this by taking the Fourier transform of the overdensity distribution. We obtain the overdensity distribution by taking the difference between the number density in the catalogue of observed galaxies and the number density in the mask.

5.1.1 Observational effects

Because we use the Hubble rate to compute distances from the measured redshifts, all our inferred distances are sensitive to the measured value of the Hubble rate. If we use a value too high, clusters of galaxies seem to be closer and smaller than they actually are. Because we assume isotropy, we assume that clustering in the radial and the angular direction should be the same. With this assumption we can correct the distances for this mistake in the projection.

Galaxies are not only flowing along the Hubble flow, but also have a peculiar velocity. A galaxy that has a peculiar velocity pointed away from us, is more redshifted than one that is at a constant comoving coordinate. Therefore these galaxies seem to be farther away naively. This causes the image of over and underdensities to become distorted. In a overdensity, where the matter is moving inwards, the nearest galaxies seem to be farther away, while the galaxies at the longest distance seem to be nearer than they actually are. This makes overdensities to look squeezed in the radial direction, while underdensities look stretched. Therefore the difference between apparent over and underdensities gets exaggerated and the power spectrum changes. We have to adjust the power spectrum for this redshift space distortion to get more accurate results.

5.2 Surveys

5.2.1 2dF Galaxy Redshift Survey

The 2-degree-Field Galaxy Redshift Survey took place between 1997 and 2002. It was conducted by the Anglo-Australian Observatory with the Anglo-Australian Telescope located in New South Wales, Australia, and includes measurements of 382,323 objects within a 1500 square degree patch of the sky, in both the north and south galactic pole regions[5].

The measurements have been used for solving many fundamental problems, *e.g.* the measurement of the power spectrum of galaxy clustering on scales up to 300 $h^{-1}\,\mathrm{Mpc}$; a new limit on the total neutrino mass, $m_{\nu,\mathrm{tot}} < 1.8\,\mathrm{eV}$; the variation in clustering properties of galaxies as functions of luminosity and spectral type.

5.2.2 Sloan Digital Sky Survey

Data collection for the Sloan Digital Sky Survey began in 2000 and the catalogue now consists of around 500 million objects covering approximately 35% of the sky. It uses a 2.5 meter wide-angle optical telescope at Apache Point Observatory in New Mexico, United States.

Its extensive period of operation can be divided in different projects. The first two, SDSS-I (2000–2005) and SDSS-II (2005–2008), included already 350 million objects. It was used to map mass distributions around galaxies (the dark matter halos) with weak gravitational lensing and for precision measurements of large scale structuring and cosmological constraints. It also measure substructures of the Milky Way and it was even used to demonstrate the common origin of dynamical asteroid families[6].

For SDSS-III (2008-2014) the spectrograph was upgraded and now it could do four surveys at the same time. It mapped the clustering of galaxies and intergalactic gas in the distant universe.

Currently SDSS-IV is taking data, it started in 2014 and is planned to run till 2020. It is extending precision measurements in the distant Universe, so for the critical early phase of cosmic history.

Chapter 6

Conclusion

The focus of this master's research was to find the effective parameters in the Effective Field Theory analytically. While familiarizing with the subject, we have encountered several difficulties which cost us too much time too reach our goal. However, we have found some new results and corrected some calculations and have learned a lot in the process. We can also sketch a path to finish what we started here.

6.1 Accomplishments

Much time was invested in understanding the calculations in the appendix of the paper by Baumann *et al.*[7]. Though the method used was clear and the initial mistake was also easy to understand, we had a hard time correcting the calculations. By knowing the end result we knew when our calculations were not yet right, but it also misguided us into looking for a magical factor while our mistake was in not including some terms. Fortunately, Daniel Baumann and Valentin Assassi immediately spotted the mistakes. Now we saw explicitly for the first time that the extra effective term cancelled the UV-divergence in P_{13}, such that we could finally conclude that the method used worked and that we could eventually use it to find the effective parameters from the analytic effective stress-energy tensor.

We have found this analytic stress-energy tensor in the Lagrangian picture of spherical collapse. Along the way we have obtained a more intuitive understanding of the spherical collapse situation. There is much to find in the literature about spherical collapse, but it was never entirely clear what were the initial conditions and what were the approximations used in the equations.

In section 4.5 we have shown that spherical collapse allows self-similar solutions. Together with the self-similarity shown in section 3.3 we can use this to find the time dependence of the effective parameters.

6.2 Outlook

It may seem that we have only obtained some disconnected results. Though we hoped that we could take all these results and wrap them in a nice final computation of the effective parameters, we could still sketch what has to be done to connect the different parts and reach a final conclusion.

First of all, we have to translate the effective stress energy tensor we have found in the Lagrangian picture to the Eulerian picture[1]. When in the familiar Eulerian coordinates, we can compute the expectation values over the short modes. With these results we can use the method in Baumann *et al.*[7] to find eventually the effective parameters of spherical collapse. Hopefully this analytic result would provide us more intuitive insight in what influences the speed of sound and viscosity of large scale structures.

[1] Enrico Pajer has already done this by now, unfortunately it was too late to include it in this thesis.

When we follow these steps, we end up with the parameters in an EdS Universe. We know our Universe is not like that and therefore we want to derive the same parameters for a ΛCDM Universe. We already switched to the easier EdS model in chapter 2, but doing all the calculations in ΛCDM should not pose real problems, because we only have to change the growth function from $D_n(a) = a^n$ to a non-trivial function. For these functions are integral representations which can be approximated as is done in *e.g.* Bernardeau *et al.*[1].

Up till now, we have totally passed over the fact that this perfect spherical symmetry only exists in the head of the theoretical physicist, rather than in the real world. It is our hope that we could find a way to divide the complex structure of the cosmic web in pieces which contain a certain symmetry approximately. This way we could build the entire universe from analytically solvable structures. This is easier said than done, because at this moment we have no idea how to add the different solutions, but we have at least one of the building blocks – or actually we think we will have one soon.

Appendix A

Calculations

Some important derivations and calculations that were too tedious for the main text are collected in this appendix.

A.1 Stress-energy tensor

In section 3.1 we introduced Gaussian smoothing. In this section we will smooth the fluid equations explicitly and derive the stress-energy tensor following Baumann *et al.*[7].

We start with the continuity equation from equation (2.7) in EdS and multiply it by the background density,

$$\partial_\tau \rho + 3\mathcal{H}\rho + \partial_i(\rho v^i) = 0. \tag{A.1}$$

Smoothing this results directly to equation (3.5),

$$\partial_\tau \rho_\ell + 3\mathcal{H}\rho_\ell + \partial_i(\rho_\ell v_\ell^i) = 0, \tag{A.2}$$

with the definitions of the long-wavelength quantities as in equations (3.2) to (3.4).

To find the effective stress-energy tensor in equation (3.6) we will smooth all the terms in the Euler equation, equation (2.8), except the stress-energy tensor σ_{ij},

$$\rho\left[\partial_\tau \boldsymbol{v} + \mathcal{H}\boldsymbol{v} + (\boldsymbol{v}\cdot\nabla)\boldsymbol{v} + \nabla\Phi\right] \tag{A.3}$$

Lets start with,

$$\text{(I)} \equiv \int_{\boldsymbol{x}'} W_\Lambda(\boldsymbol{x}-\boldsymbol{x}')\bar{\rho}(\tau)\left(1+\delta(\boldsymbol{x}',\tau)\right)\left[\partial_\tau v^i(\boldsymbol{x}',\tau) + \mathcal{H}v^i(\boldsymbol{x}',\tau) + v^j\nabla_j v^i\right] \tag{A.4}$$

$$= \left(\partial_\tau + 4\mathcal{H}\right)[\rho_\ell v_\ell^i](\boldsymbol{x}) + \int_{\boldsymbol{x}'} W_\Lambda(\boldsymbol{x}-\boldsymbol{x}')\left[v^i\partial_j[\rho v^j] + v^j\rho\partial_j v^i\right] \tag{A.5}$$

where we have used the continuity equation, $\partial_\tau\delta = -\partial_i[(1+\delta)v^i]$. We can use partial integration and $\partial_{i'}W(\boldsymbol{x}-\boldsymbol{x}') = -\partial_i W(\boldsymbol{x}-\boldsymbol{x}')$ in the last term,

$$\text{(I)} = \left(\partial_\tau + 4\mathcal{H}\right)[\rho_\ell v_\ell^i](\boldsymbol{x}) + \partial_j\int_{\boldsymbol{x}'} W_\Lambda(\boldsymbol{x}-\boldsymbol{x}')\rho v^i v^j. \tag{A.6}$$

We define

$$\boldsymbol{v} \equiv \boldsymbol{v}_\ell + \boldsymbol{v}_\mathrm{s}, \tag{A.7}$$

and Taylor expand $\boldsymbol{v}_\ell(\boldsymbol{x}')$ around $\boldsymbol{x}$,

$$\boldsymbol{v}_\ell(\boldsymbol{x}') = \boldsymbol{v}_\ell(\boldsymbol{x}) + (\boldsymbol{x}-\boldsymbol{x}')^i\partial_i\boldsymbol{v}_\ell(\boldsymbol{x}) + \frac{1}{2}(\boldsymbol{x}-\boldsymbol{x}')^i(\boldsymbol{x}-\boldsymbol{x}')^j\partial_i\partial_j\boldsymbol{v}_\ell(\boldsymbol{x}) + \ldots. \tag{A.8}$$

We want to compute

$$\left[\rho v^i v^j\right]_\Lambda = \left[\rho v_\ell^i v_\ell^j\right]_\Lambda + 2\left[\rho v_\ell^{(i} v_{\rm s}^{j)}\right]_\Lambda + \left[\rho v_{\rm s}^i v_{\rm s}^j\right]_\Lambda \tag{A.9}$$

From the definition of the Gaussian filter, we have

$$\partial_{i'} W_\Lambda(\boldsymbol{x}-\boldsymbol{x}') = -\partial_i W_\Lambda(\boldsymbol{x}-\boldsymbol{x}') = \Lambda^2(\boldsymbol{x}-\boldsymbol{x}')^i W_\Lambda(\boldsymbol{x}-\boldsymbol{x}'), \tag{A.10}$$

$$\begin{aligned}\partial_{i'}\partial_{j'} W_\Lambda(\boldsymbol{x}-\boldsymbol{x}') &= \partial_i\partial_j W_\Lambda(\boldsymbol{x}-\boldsymbol{x}') \\ &= -\Lambda^2\delta_{ij} W_\Lambda(\boldsymbol{x}-\boldsymbol{x}') + \Lambda^4(\boldsymbol{x}-\boldsymbol{x}')^i(\boldsymbol{x}-\boldsymbol{x}')^j W_\Lambda(\boldsymbol{x}-\boldsymbol{x}'),\end{aligned} \tag{A.11}$$

and using equation (A.8),

$$\begin{aligned}v_\ell^i(\boldsymbol{x}')v_\ell^j(\boldsymbol{x}') = v_\ell^i(\boldsymbol{x})v_\ell^j(\boldsymbol{x}) &+ 2v_\ell^{(i}\partial_k v_\ell^{j)}(\boldsymbol{x}-\boldsymbol{x}')^k \\ &+ \left[v_\ell^{(i}\partial_k\partial_l v_\ell^{j)} + \partial_k v_\ell^i \partial_l v_\ell^j\right](\boldsymbol{x}-\boldsymbol{x}')^k(\boldsymbol{x}-\boldsymbol{x}')^l + \dots,\end{aligned} \tag{A.12}$$

we can find the first term of equation (A.9),

$$\begin{aligned}\left[\rho v_\ell^i v_\ell^j\right]_\Lambda &= \rho_\ell v_\ell^i v_\ell^j - \frac{2}{\Lambda^2} v_\ell^{(i}\partial_k v_\ell^{j)}\partial_k\rho_\ell + \left[v_\ell^{(i}\partial_k\partial_l v_\ell^{j)} + \partial_k v_\ell^i\partial_l v_\ell^j\right]\times\left[\frac{1}{\Lambda^4}\partial_k\partial_l\rho_\ell + \frac{1}{\Lambda^2}\delta_{kl}\rho_\ell\right] + \dots \\ &= \rho_\ell v_\ell^i v_\ell^j - \frac{2}{\Lambda^2} v_\ell^{(i}\partial_k v_\ell^{j)}\partial_k\rho_\ell + \frac{1}{\Lambda^2}\rho_\ell v_\ell^{(i}\partial^2 v_\ell^{j)} + \frac{1}{\Lambda^2}\rho_\ell\partial_k v_\ell^i\partial_k v_\ell^j + \text{h.o. derivatives}\end{aligned} \tag{A.13}$$

Before we compute the second term of equation (A.9), we look at

$$\begin{aligned}\left[\rho v_{\rm s}^i\right]_\Lambda &= \left[\rho v^i\right]_\Lambda - \left[\rho v_\ell^i\right]_\Lambda \\ &= \frac{1}{\Lambda^2}\partial_k v_\ell^i\partial_k\rho_\ell - \frac{1}{2\Lambda^2}\rho_\ell\partial^2 v_\ell^i,\end{aligned} \tag{A.14}$$

Because this has only terms of second order in derivatives we get,

$$2\left[\rho v_\ell^{(i} v_{\rm s}^{j)}\right]_\Lambda = \frac{2}{\Lambda^2} v_\ell^{(i}\partial_k v_\ell^{j)}\partial_k\rho_\ell - \frac{1}{\Lambda^2}\rho_\ell v_\ell^{(i}\partial^2 v_\ell^{j)} + \text{h.o. derivatives}, \tag{A.15}$$

and thus,

$$\left[\rho v^i v^j\right]_\Lambda = \rho_\ell v_\ell^i v_\ell^j + \left[\rho v_{\rm s}^i v_{\rm s}^j\right]_\Lambda + \frac{1}{\Lambda^2}\rho_\ell\partial_k v_\ell^i\partial_k v_\ell^j. \tag{A.16}$$

With the use of the smoothed continuity equation (A.2), we finally get

$$\text{(I)} = \rho_\ell\partial_\tau v_\ell^i + \mathcal{H}\rho_\ell v_\ell^i + \rho_\ell v_\ell^j\partial_j v_\ell^i + \partial_j\left[\rho v_{\rm s}^i v_{\rm s}^j\right]_\Lambda + \mathcal{C}^{ij}, \tag{A.17}$$

with

$$\mathcal{C}^{ij} = \frac{1}{\Lambda^2}\rho_\ell\partial_k v_\ell^i\partial_k v_\ell^j \tag{A.18}$$

Now we want to smooth the last term of equation (2.8),

$$\text{(II)} \equiv \left[\rho\partial_i\Phi\right]_\Lambda = \left[\rho_\ell\partial_i\phi_\ell\right]_\Lambda + \left[\rho_{\rm s}\partial_i\phi_\ell\right]_\Lambda + \left[\rho_\ell\partial_i\phi_{\rm s}\right]_\Lambda + \left[\rho_{\rm s}\partial_i\phi_{\rm s}\right]_\Lambda. \tag{A.19}$$

We split the density and the Newtonian potential in long and short modes,

$$\rho \equiv \rho_\ell + \rho_{\rm s}, \qquad \Phi \equiv \phi_\ell + \phi_{\rm s}, \qquad \text{with} \quad \phi_\ell \equiv \left[\phi\right]_\Lambda \tag{A.20}$$

Again we can expand these long modes around $\boldsymbol{x}$ and get,

$$\left[\rho_{\rm s}\right]_\Lambda = -\frac{1}{2\Lambda^2}\partial^2\rho_\ell, \qquad \left[\phi_{\rm s}\right]_\Lambda = -\frac{1}{2\Lambda^2}\partial^2\phi_\ell. \tag{A.21}$$

and from there,

$$(\mathrm{II}) = \rho_\ell \partial_i \phi_\ell + [\rho_\mathrm{s} \partial_i \phi_\mathrm{s}]_\Lambda + \frac{1}{\Lambda^2} \partial_i \partial_k \phi_\ell \partial_k \rho_\ell. \tag{A.22}$$

Using the Poisson equation for the small modes, $\partial^2 \phi_\mathrm{s} = 4\pi G \rho_\mathrm{s}$, partial integration and $\partial_{i'} W_\Lambda = -\partial_i W_\Lambda$, we get,

$$\begin{aligned}
[\rho_\mathrm{s} \partial_i \phi_\mathrm{s}]_\Lambda &= \frac{1}{4\pi G} \left[\partial^2 \phi_\mathrm{s} \partial_i \phi_\mathrm{s}\right]_\Lambda = \frac{1}{4\pi G} \left[\partial_j \left(\partial_j \phi_\mathrm{s} \partial_i \phi_\mathrm{s}\right) - \frac{1}{2} \partial_i \left(\partial_j \phi_\mathrm{s} \partial_j \phi_\mathrm{s}\right)\right]_\Lambda \\
&= \frac{1}{4\pi G} \partial_j \left[\partial_j \phi_\mathrm{s} \partial_i \phi_\mathrm{s}\right]_\Lambda - \frac{1}{8\pi G} \partial_i \left[\partial_j \phi_\mathrm{s} \partial_j \phi_\mathrm{s}\right]_\Lambda \\
&= \partial_j \left[\frac{2 \partial_i \phi_\mathrm{s} \partial_j \phi_\mathrm{s} - \delta_{ij} \partial_k \phi_\mathrm{s} \partial_k \phi_\mathrm{s}}{8\pi G}\right]_\Lambda,
\end{aligned} \tag{A.23}$$

and if we use the long mode part of the Poisson equation, $\partial^2 \phi_\ell = 4\pi G \rho_\ell$,we can rewrite the last term of equation (A.22) as well,

$$\left(\partial_i \partial_k \phi_\ell\right) \left(\partial_k \phi_\ell\right) = \frac{1}{4\pi G} \left(\partial_i \partial_k \phi_\ell\right) \left(\partial_k \partial^2 \rho_\ell\right) \tag{A.24}$$

$$\begin{aligned}
&= \frac{1}{4\pi G} \partial_j \left[\left(\partial_i \partial_k \phi_\ell\right) \left(\partial_j \partial_k \rho_\ell\right)\right] - \frac{1}{8\pi G} \partial_i \left[\left(\partial_j \partial_k \phi_\ell\right) \left(\partial_j \partial_k \phi_\ell\right)\right] \\
&= \partial_j \left[\frac{2 \left(\partial_i \partial_k \phi_\ell\right) \left(\partial_j \partial_k \rho_\ell\right) - \delta_{ij} \left(\partial_k \partial_l \phi_\ell\right) \left(\partial_k \partial_l \phi_\ell\right)}{8\pi G}\right] \equiv \partial_j \mathcal{D}^{ij}.
\end{aligned} \tag{A.25}$$

Hence,

$$(\mathrm{II}) = \rho_\ell \partial_i \phi_\ell + \partial_j \left[\frac{2 \partial_j \phi_\mathrm{s} \partial_i \phi_\mathrm{s} - \delta_{ij} \partial_k \phi_\mathrm{s} \partial_k \phi_\mathrm{s}}{8\pi G}\right]_\Lambda + \partial_j \mathcal{D}^{ij} \tag{A.26}$$

Summing the results of equations (A.17) and (A.26), we get the smoothed Euler equation,

$$\begin{gathered}
(\mathrm{I}) + (\mathrm{II}) = 0 \\
\rho_\ell \partial_\tau v_\ell^i + \mathcal{H} \rho_\ell v_\ell^i + \rho_\ell v_\ell^j \partial_j \boldsymbol{\ell}^i + \rho_\ell \partial_i \phi_\ell = -\partial_j \left[\tau^{ij}\right]_\Lambda - \partial_j \tau^{ij}_{\partial^2},
\end{gathered} \tag{A.27}$$

with the stress-energy tensor

$$\tau^{ij} = \rho v_\mathrm{s}^i v_\mathrm{s}^j - \frac{\delta_{ij} \partial_k \phi_\mathrm{s} \partial_k \phi_\mathrm{s} - 2 \partial_i \phi_\mathrm{s} \partial_j \phi_\mathrm{s}}{8\pi G} \tag{A.28}$$

and

$$\tau^{ij}_{\partial^2} = \mathcal{C}^{ij} + \mathcal{D}^{ij} \tag{A.29}$$

which is second order in derivatives.

A.2 Effective paramaters in perturbation theory

The parameters of the effective field theory can be computed using expectation values as is shown in section 3.2,

$$\bar{p}_\mathrm{eff} = \frac{1}{3} \lim_{k \to 0} \langle \tau \rangle, \quad c_s^2 + c_\mathrm{bv}^2 = \frac{1}{\bar{\rho}} \frac{\langle \delta_\ell p_\mathrm{eff} \rangle}{\langle \delta_\ell \delta_\ell \rangle}, \quad c_\mathrm{sv}^2 = \frac{\langle \delta_\ell \sigma_\mathrm{eff} \rangle}{\langle \delta_\ell \delta_\ell \rangle}, \quad \text{with } \sigma_\mathrm{eff} = \frac{1}{\bar{\rho}} \frac{\partial_i \partial_j}{\partial^2} \langle [\hat{\tau}^i{}_j]^\Lambda \rangle. \tag{A.30}$$

The explicit calculation was already attempted by Baumann *et al.*[7], but we found some mistakes in that calculation. With the help of Daniel Baumann and Valentin Assassi, we have managed to fix these mistakes and found the satisfying results below.

We want to compute $c_{\rm s}^2$ and $c_{\rm sv}^2$ up to the lowest order in perturbation theory. When we look at the non-perturbative stress-energy tensor in equation (3.7) we see that we can write

$$\tau_{ij} = \tau_{ij}^{(2)} + \tau_{ij}^{(3)} + \dots, \tag{A.31}$$

where $\tau_{ij}^{(n)}$ is n-th order in $\delta^{(1)}$. We are not interested in $\bar{p}_{\rm eff}$ and $\sigma_{\rm eff}$ but only want to calculate the speed of sound and the viscosity. Because δ_ℓ is only first order in $\delta^{(1)}$, and correlation functions over odd numbers of linear perturbations vanish, we are only interested in

$$\begin{aligned}\tau_{ij}^{(3)} &\equiv \bar{\rho}\left(\delta^{(1)}v_i^{(1)}v_j^{(1)} + v_i^{(1)}v_j^{(2)} + v_i^{(2)}v_j^{(1)}\right) \\ &\quad - \frac{2\bar{\rho}}{3\mathcal{H}^2}\left(\delta_{ij}\partial_k\phi^{(1)}\partial_k\phi^{(2)} - \partial_i\phi^{(1)}\partial_j\phi^{(2)} - \partial_i\phi^{(2)}\partial_j\phi^{(1)}\right), \end{aligned}\tag{A.32}$$

$$\tau^{(3)} \equiv \bar{\rho}\delta^{(1)}\boldsymbol{v}^{(1)}\cdot\boldsymbol{v}^{(1)} + 2\bar{\rho}\boldsymbol{v}^{(1)}\cdot\boldsymbol{v}^{(2)} - \frac{2\bar{\rho}}{3\mathcal{H}^2}\partial_k\phi^{(1)}\partial_k\phi^{(2)}. \tag{A.33}$$

If we assume we can write $v_i(\boldsymbol{x}) = \partial_i u(\boldsymbol{x})$, then we can use

$$\boldsymbol{v}_{\boldsymbol{k}}^{(n)} = -\frac{\mathrm{i}\boldsymbol{k}}{k^2}\theta_{\boldsymbol{k}}^{(n)}, \tag{A.34}$$

to rewrite the first two terms in equation (A.33). For the third term, we use Poisson's equation,

$$\partial^2\phi(\boldsymbol{x}) = 4\pi G a^2\bar{\rho}\delta(\boldsymbol{x}), \qquad \text{and thus} \qquad \phi_{\boldsymbol{k}}^{(n)} = -\frac{3\mathcal{H}^2}{2k^2}\delta_{\boldsymbol{k}}^{(n)}, \tag{A.35}$$

and fill this in

$$\left[\tau^{(3)}\right]_\Lambda(\boldsymbol{p}) = W_\Lambda(p)\int_{\boldsymbol{x}}\tau^{(3)}(\boldsymbol{x})\mathrm{e}^{-\mathrm{i}\boldsymbol{p}\cdot\boldsymbol{x}} \tag{A.36}$$

$$\begin{aligned}&= 2\bar{\rho}W_\Lambda(p)\int_{\boldsymbol{x}}\int_{\boldsymbol{k}}\int_{\boldsymbol{q}}\mathrm{e}^{-\mathrm{i}(\boldsymbol{p}-\boldsymbol{k}-\boldsymbol{q})\cdot\boldsymbol{x}}\left[\boldsymbol{v}_{\boldsymbol{k}}^{(1)}\cdot\boldsymbol{v}_{\boldsymbol{q}}^{(2)} - \frac{1}{3\mathcal{H}^2}(\mathrm{i}\boldsymbol{k})\cdot(\mathrm{i}\boldsymbol{q})\phi_{\boldsymbol{k}}^{(1)}\phi_{\boldsymbol{q}}^{(2)}\right] \\ &\quad + \bar{\rho}W_\Lambda(p)\int_{\boldsymbol{x}}\int_{\boldsymbol{q}}\int_{\boldsymbol{q}_1}\int_{\boldsymbol{q}_2}\mathrm{e}^{-\mathrm{i}(\boldsymbol{p}-\boldsymbol{q}-\boldsymbol{q}_1-\boldsymbol{q}_2)\cdot\boldsymbol{x}}\delta_{\boldsymbol{q}}^{(1)}\boldsymbol{v}_{\boldsymbol{q}_1}^{(1)}\cdot\boldsymbol{v}_{\boldsymbol{q}_2}^{(1)}\end{aligned}\tag{A.37}$$

$$\begin{aligned}&= 2\bar{\rho}W_\Lambda(p)\int_{\boldsymbol{q}}\alpha(\boldsymbol{q},\boldsymbol{p})\left[-\theta_{\boldsymbol{p}-\boldsymbol{q}}^{(1)}\theta_{\boldsymbol{q}}^{(2)} + \frac{3\mathcal{H}^2}{4}\delta_{\boldsymbol{p}-\boldsymbol{q}}^{(1)}\delta_{\boldsymbol{q}}^{(2)}\right] \\ &\quad - \bar{\rho}W_\Lambda(p)\int_{\boldsymbol{q}}\int_{\boldsymbol{q}_1}\int_{\boldsymbol{q}_2}\frac{\boldsymbol{q}_1\cdot\boldsymbol{q}_2}{q_1^2q_2^2}\delta_{\boldsymbol{p}-\boldsymbol{q}}^{(1)}\theta_{\boldsymbol{q}_1}^{(1)}\theta_{\boldsymbol{q}_2}^{(1)}\delta_D(\boldsymbol{q}-\boldsymbol{q}_1-\boldsymbol{q}_2)\end{aligned}\tag{A.38}$$

$$\begin{aligned}&= -\frac{1}{2}\bar{\rho}\mathcal{H}^2W_\Lambda(p)\int_{\boldsymbol{q}}\int_{\boldsymbol{q}_1}\int_{\boldsymbol{q}_2}\alpha(\boldsymbol{q},\boldsymbol{p})H_2(\boldsymbol{q}_1,\boldsymbol{q}_2)\delta_{\boldsymbol{p}-\boldsymbol{q}}^{(1)}\delta_{\boldsymbol{q}_1}^{(1)}\delta_{\boldsymbol{q}_2}^{(1)}\delta_D(\boldsymbol{q}-\boldsymbol{q}_1-\boldsymbol{q}_2) \\ &\quad - \bar{\rho}\mathcal{H}^2W_\Lambda(p)\int_{\boldsymbol{q}}\int_{\boldsymbol{q}_1}\int_{\boldsymbol{q}_2}\frac{\boldsymbol{q}_1\cdot\boldsymbol{q}_2}{q_1^2q_2^2}\delta_{\boldsymbol{p}-\boldsymbol{q}}^{(1)}\delta_{\boldsymbol{q}_1}^{(1)}\delta_{\boldsymbol{q}_2}^{(1)}\delta_D(\boldsymbol{q}-\boldsymbol{q}_1-\boldsymbol{q}_2)\end{aligned}\tag{A.39}$$

where

$$\alpha(\boldsymbol{q},\boldsymbol{p}) = \frac{(\boldsymbol{p}-\boldsymbol{q})\cdot\boldsymbol{q}}{(\boldsymbol{p}-\boldsymbol{q})^2q^2}, \tag{A.40}$$

and

$$H_2(\boldsymbol{q}_1,\boldsymbol{q}_2) = 4G_2(\boldsymbol{q}_1,\boldsymbol{q}_2) - 3F_2(\boldsymbol{q}_1,\boldsymbol{q}_2) = -\frac{3}{7} + \frac{1}{2}\mu\left(\frac{q_1}{q_2}+\frac{q_2}{q_1}\right) + \frac{10}{7}. \tag{A.41}$$

We want to compute

$$\begin{aligned}\langle\delta_{\boldsymbol{k}}^{(1)}[\tau]_{\boldsymbol{p}}^\Lambda\rangle &= -\frac{1}{2}\bar{\rho}\mathcal{H}^2W_\Lambda(p)\int_{\boldsymbol{q}}\int_{\boldsymbol{q}_1}\int_{\boldsymbol{q}_2}\alpha(\boldsymbol{q},\boldsymbol{p})H_2(\boldsymbol{q}_1,\boldsymbol{q}_2)\delta_D(\boldsymbol{q}-\boldsymbol{q}_1-\boldsymbol{q}_2)\langle\delta_{\boldsymbol{k}}^{(1)}\delta_{\boldsymbol{p}-\boldsymbol{q}}^{(1)}\delta_{\boldsymbol{q}_1}^{(1)}\delta_{\boldsymbol{q}_2}^{(1)}\rangle. \\ &\quad - \bar{\rho}\mathcal{H}^2W_\Lambda(p)\int_{\boldsymbol{q}}\int_{\boldsymbol{q}_1}\int_{\boldsymbol{q}_2}\frac{\boldsymbol{q}_1\cdot\boldsymbol{q}_2}{q_1^2q_2^2}\delta_D(\boldsymbol{q}-\boldsymbol{q}_1-\boldsymbol{q}_2)\langle\delta_{\boldsymbol{k}}^{(1)}\delta_{\boldsymbol{p}-\boldsymbol{q}}^{(1)}\delta_{\boldsymbol{q}_1}^{(1)}\delta_{\boldsymbol{q}_2}^{(1)}\rangle.\end{aligned}\tag{A.42}$$

Therefore we will look first at

$$\langle \delta^{(1)}_{\boldsymbol{k}} \delta^{(1)}_{\boldsymbol{p}-\boldsymbol{q}} \delta^{(1)}_{\boldsymbol{q}_1} \delta^{(1)}_{\boldsymbol{q}_2} \rangle = \langle \delta^{(1)}_{\boldsymbol{k}} \delta^{(1)}_{\boldsymbol{p}-\boldsymbol{q}} \rangle \langle \delta^{(1)}_{\boldsymbol{q}_1} \delta^{(1)}_{\boldsymbol{q}_2} \rangle + \langle \delta^{(1)}_{\boldsymbol{k}} \delta^{(1)}_{\boldsymbol{q}_1} \rangle \langle \delta^{(1)}_{\boldsymbol{p}-\boldsymbol{q}} \delta^{(1)}_{\boldsymbol{q}_2} \rangle + \langle \delta^{(1)}_{\boldsymbol{k}} \delta^{(1)}_{\boldsymbol{q}_2} \rangle \langle \delta^{(1)}_{\boldsymbol{p}-\boldsymbol{q}} \delta^{(1)}_{\boldsymbol{q}_1} \rangle$$

$$= \delta_D(\boldsymbol{k}+\boldsymbol{p}-\boldsymbol{q}) \delta_D(\boldsymbol{q}_1+\boldsymbol{q}_2) P_\delta(k) P_\delta(q_1) \tag{A.43}$$

$$+ \delta_D(\boldsymbol{k}+\boldsymbol{q}_1) \delta_D(\boldsymbol{p}-\boldsymbol{q}+\boldsymbol{q}_2) P_\delta(k) P_\delta(|\boldsymbol{p}-\boldsymbol{q}|) \tag{A.44}$$

$$+ \delta_D(\boldsymbol{k}+\boldsymbol{q}_2) \delta_D(\boldsymbol{p}-\boldsymbol{q}+\boldsymbol{q}_1) P_\delta(k) P_\delta(|\boldsymbol{p}-\boldsymbol{q}|) \tag{A.45}$$

Because $H_2(\boldsymbol{q}_1, \boldsymbol{q}_2)$ is symmetric, the first term will vanish under the integral in equation (A.42) while the last two give the same. We can now compute the integrals over $\boldsymbol{q}_1$ and $\boldsymbol{q}_2$

$$\int_{\boldsymbol{q}_1} \int_{\boldsymbol{q}_2} H_2(\boldsymbol{q}_1, \boldsymbol{q}_2) \delta_D(\boldsymbol{q}-\boldsymbol{q}_1-\boldsymbol{q}_2) \langle \delta^{(1)}_{\boldsymbol{k}} \delta^{(1)}_{\boldsymbol{p}-\boldsymbol{q}} \delta^{(1)}_{\boldsymbol{q}_1} \delta^{(1)}_{\boldsymbol{q}_2} \rangle$$

$$= 2\delta_D(\boldsymbol{p}+\boldsymbol{k}) P_\delta(k) H_2(-\boldsymbol{k}, \boldsymbol{k}+\boldsymbol{q}) P_\delta(|\boldsymbol{p}-\boldsymbol{q}|)$$

$$+ \delta_D(\boldsymbol{q}) \delta(\boldsymbol{p}+\boldsymbol{k}) P_\delta(k) \int_{\boldsymbol{q}'} H_2(\boldsymbol{q}', -\boldsymbol{q}') P_\delta(\boldsymbol{q}')$$

$$= 2\langle \delta^{(1)}_{\boldsymbol{k}} \delta^{(1)}_{\boldsymbol{p}} \rangle H_2(-\boldsymbol{k}, \boldsymbol{k}+\boldsymbol{q}) P_\delta(|\boldsymbol{p}-\boldsymbol{q}|)$$

$$+ \langle \delta^{(1)}_{\boldsymbol{k}} \delta^{(2)}_{\boldsymbol{p}} \rangle \delta_D(q) \int_{\boldsymbol{q}'} H_2(\boldsymbol{q}', -\boldsymbol{q}') P_\delta(\boldsymbol{q}'), \tag{A.46}$$

$$\int_{\boldsymbol{q}_1} \int_{\boldsymbol{q}_2} \frac{\boldsymbol{q}_1 \cdot \boldsymbol{q}_2}{q_1^2 q_2^2} \delta_D(\boldsymbol{q}-\boldsymbol{q}_1-\boldsymbol{q}_2) \langle \delta^{(1)}_{\boldsymbol{k}} \delta^{(1)}_{\boldsymbol{p}-\boldsymbol{q}} \delta^{(1)}_{\boldsymbol{q}_1} \delta^{(1)}_{\boldsymbol{q}_2} \rangle$$

$$= -2\alpha(\boldsymbol{p}, \boldsymbol{q}) \delta_D(\boldsymbol{p}+\boldsymbol{k}) P_\delta(k) P_\delta(|\boldsymbol{p}-\boldsymbol{q}|)$$

$$- \delta_D(q) \delta_D(\boldsymbol{p}+\boldsymbol{k}) P_\delta(k) \int_{\boldsymbol{q}'} \frac{1}{q'^2} P_\delta(q') \tag{A.47}$$

$$= -2\langle \delta^{(1)}_{\boldsymbol{k}} \delta^{(1)}_{\boldsymbol{p}} \rangle \alpha(\boldsymbol{p}, \boldsymbol{q}) P_\delta(|\boldsymbol{p}-\boldsymbol{q}|)$$

$$- \langle \delta^{(1)}_{\boldsymbol{k}} \delta^{(1)}_{\boldsymbol{p}} \rangle \delta_D(q) \int_{\boldsymbol{q}'} \frac{1}{q'^2} P_\delta(q') \tag{A.48}$$

and insert this in equation (A.42)

$$\langle \delta^{(1)}_{\boldsymbol{k}}[\tau]^\Lambda_{\boldsymbol{p}} \rangle = -\bar{\rho}\mathcal{H}^2 W_\Lambda(k) \langle \delta^{(1)}_{\boldsymbol{k}} \delta^{(1)}_{\boldsymbol{p}} \rangle \int_{\boldsymbol{q}} \left\{ \alpha(\boldsymbol{q}, -\boldsymbol{k}) H_2(-\boldsymbol{k}, \boldsymbol{k}+\boldsymbol{q}) - 2\alpha(-\boldsymbol{k}, \boldsymbol{q}) \right\} P_\delta(|\boldsymbol{k}+\boldsymbol{q}|)$$

$$- \frac{1}{2} \bar{\rho}\mathcal{H}^2 W_\Lambda(k) \langle \delta^{(1)}_{\boldsymbol{k}} \delta^{(1)}_{\boldsymbol{p}} \rangle \int_{\boldsymbol{q}} \left[H_2(\boldsymbol{q}, -\boldsymbol{q}) - \frac{2}{q^2} \right] P_\delta(q) \tag{A.49}$$

$$= -\bar{\rho}\mathcal{H}^2 W_\Lambda(k) \langle \delta^{(1)}_{\boldsymbol{k}} \delta^{(1)}_{\boldsymbol{p}} \rangle \int_{\boldsymbol{q}} \left\{ \alpha(\boldsymbol{q}-\boldsymbol{k}, -\boldsymbol{k}) H_2(-\boldsymbol{k}, \boldsymbol{q}) - 2\alpha(-\boldsymbol{k}, \boldsymbol{q}-\boldsymbol{k}) \right\} P_\delta(q)$$

$$+ \bar{\rho}\mathcal{H}^2 W_\Lambda(k) \langle \delta^{(1)}_{\boldsymbol{k}} \delta^{(1)}_{\boldsymbol{p}} \rangle \int_{\boldsymbol{q}} \frac{1}{q^2} P_\delta(q) \tag{A.50}$$

$$= -\bar{\rho}\mathcal{H}^2 W_\Lambda(k) \langle \delta^{(1)}_{\boldsymbol{k}} \delta^{(1)}_{\boldsymbol{p}} \rangle \int_{\boldsymbol{q}} \Bigg\{ \alpha(\boldsymbol{q}-\boldsymbol{k}, -\boldsymbol{k}) H_2(-\boldsymbol{k}, \boldsymbol{q}) \tag{A.51}$$

$$- 2\alpha(-\boldsymbol{k}, \boldsymbol{q}-\boldsymbol{k}) - \frac{1}{q^2} \Bigg\} P_\delta(q) \tag{A.52}$$

To compute c_s^2, we have to take the limit $k \ll q$. We expand around $k = 0$,

$$\alpha(\boldsymbol{q}-\boldsymbol{k}, -\boldsymbol{k}) H_2(-\boldsymbol{k}, \boldsymbol{q}) - 2\alpha(-\boldsymbol{k}, \boldsymbol{q}-\boldsymbol{k}) - \frac{1}{q^2}$$

$$= \left[-\frac{1}{q^2} - \mu \frac{k}{q^3} + \mathcal{O}\left(k^2\right) \right] \times \left[-\frac{3}{7} - \frac{1}{2}\mu \frac{q}{k} + \frac{10}{7}\mu^2 + \mathcal{O}\left(k\right) \right] - 2\mu \frac{1}{kq} - \frac{1}{q^2}$$

$$= -\frac{1}{q^2} \left(\frac{4}{7} + \frac{13}{14}\mu^2 + \mathcal{O}\left(k\right) \right) + \text{terms linear in } \mu \tag{A.53}$$

with now

$$\mu = \frac{\boldsymbol{k}\cdot\boldsymbol{q}}{kq}$$

and hence the integral in equation (A.52) becomes

$$\begin{aligned} c_s^2 + c_{\rm bv}^2 &= \frac{1}{3\bar{\rho}}\frac{\langle \delta^{(1)}_{\boldsymbol{k}}[\tau]^{\Lambda}_{\boldsymbol{p}}\rangle}{\langle \delta^{(1)}_{\boldsymbol{k}}\delta^{(1)}_{\boldsymbol{p}}\rangle} = \frac{1}{3}\mathcal{H}^2\int_{\boldsymbol{q}}\frac{1}{q^2}\left(\frac{4}{7}+\frac{13}{14}\mu^2\right)P_\delta(q) \\ &= \frac{1}{3}\frac{1}{(2\pi)^2}\mathcal{H}^2\int \mathrm{d}q\, P_\delta(q)\int_{-1}^{1}\mathrm{d}\mu\left(\frac{4}{7}+\frac{13}{14}\mu^2\right) \qquad \text{(A.54)} \\ &= \frac{37}{126}\frac{1}{2\pi^2}\mathcal{H}^2\int \mathrm{d}q\, P_\delta(q) \qquad \text{(A.55)} \end{aligned}$$

While $\theta^{(1)}_{\boldsymbol{k}} = -\mathcal{H}\delta^{(1)}_{\boldsymbol{k}}$ holds for the first order, for the second order $\theta^{(2)}_{\boldsymbol{k}} \neq -\mathcal{H}\delta^{(2)}_{\boldsymbol{k}}$. This is the reason why we get the $H_2(\boldsymbol{k},\boldsymbol{q})$ in the previous expression, instead of $F_2(\boldsymbol{k},\boldsymbol{q})$ in [7], and thus this also explains the difference in the end result.

For $c_{\rm sv}^2$ we follow the same steps, starting from equation (A.32),

$$\begin{aligned} \left[\hat{\tau}^{(3)}_{ij}\right]_\Lambda(\boldsymbol{p}) &= W_\Lambda(p)\int_{\boldsymbol{k}}\int_{\boldsymbol{q}}\left\{\bar{\rho}\left(\left(v^{(1)}_{\boldsymbol{k}}\right)_i\left(v^{(2)}_{\boldsymbol{q}}\right)_j + \left(v^{(2)}_{\boldsymbol{k}}\right)_i\left(v^{(1)}_{\boldsymbol{q}}\right)_j - \frac{2}{3}\delta_{ij}\boldsymbol{v}^{(1)}_{\boldsymbol{k}}\cdot\boldsymbol{v}^{(2)}_{\boldsymbol{q}}\right)\right. \\ &\quad \left. + \frac{2\bar{\rho}}{3\mathcal{H}^2}\left(\frac{2}{3}\delta_{ij}(\boldsymbol{k}\cdot\boldsymbol{q}) - k_iq_j - k_jq_i\right)\phi^{(1)}_{\boldsymbol{k}}\phi^{(2)}_{\boldsymbol{q}}\right\}\delta_D(\boldsymbol{p}-\boldsymbol{q}-\boldsymbol{k}) \\ &\quad + W_\Lambda(p)\bar{\rho}\int_{\boldsymbol{q}}\int_{\boldsymbol{q}_1}\int_{\boldsymbol{q}_2}\left\{\delta^{(1)}_{\boldsymbol{q}}\left(v^{(1)}_{\boldsymbol{q}_1}\right)_i\left(v^{(1)}_{\boldsymbol{q}_1}\right)_j - \frac{1}{3}\delta_{ij}\delta^{(1)}_{\boldsymbol{q}}\boldsymbol{v}^{(1)}_{\boldsymbol{q}_1}\cdot\boldsymbol{v}^{(1)}_{\boldsymbol{q}_2}\right\}\delta_D(\boldsymbol{p}-\boldsymbol{q}-\boldsymbol{q}_1-\boldsymbol{q}_2) \qquad \text{(A.56)} \\ &= -2\bar{\rho}W_\Lambda(p)\int_{\boldsymbol{q}}\left\{\frac{(p_i-q_i)q_j - \frac{1}{3}\delta_{ij}(\boldsymbol{p}-\boldsymbol{q})\cdot\boldsymbol{q}}{(\boldsymbol{p}-\boldsymbol{q})^2q^2}\left(\theta^{(1)}_{\boldsymbol{p}-\boldsymbol{q}}\theta^{(2)}_{\boldsymbol{q}} + \frac{3\mathcal{H}^2}{2}\delta^{(1)}_{\boldsymbol{p}-\boldsymbol{q}}\delta^{(2)}_{\boldsymbol{q}}\right)\right\} \\ &\quad + W_\Lambda(p)\bar{\rho}\int_{\boldsymbol{q}}\int_{\boldsymbol{q}_1}\int_{\boldsymbol{q}_2}\frac{q_1^iq_2^j - \frac{1}{3}\delta_{ij}\boldsymbol{q}_1\cdot\boldsymbol{q}_2}{q_1^2q_2^2}\delta^{(1)}_{\boldsymbol{q}}\theta^{(1)}_{\boldsymbol{q}_1}\theta^{(1)}_{\boldsymbol{q}_2}\delta_D(\boldsymbol{p}-\boldsymbol{q}-\boldsymbol{q}_1-\boldsymbol{q}_2) \qquad \text{(A.57)} \\ &= -5\bar{\rho}\mathcal{H}^2W_\Lambda(p)\int_{\boldsymbol{q}}\int_{\boldsymbol{q}_1}\int_{\boldsymbol{q}_2}\beta_{ij}(\boldsymbol{q},\boldsymbol{p})\tilde{H}_2(\boldsymbol{q}_1,\boldsymbol{q}_2)\delta^{(1)}_{\boldsymbol{p}-\boldsymbol{q}}\delta^{(1)}_{\boldsymbol{q}_1}\delta^{(1)}_{\boldsymbol{q}_2} \\ &\quad + \bar{\rho}\mathcal{H}^2W_\Lambda(p)\int_{\boldsymbol{q}}\int_{\boldsymbol{q}_1}\int_{\boldsymbol{q}_2}\frac{q_1^iq_2^j - \frac{1}{3}\delta_{ij}\boldsymbol{q}_1\cdot\boldsymbol{q}_2}{q_1^2q_2^2}\delta^{(1)}_{\boldsymbol{q}}\delta^{(1)}_{\boldsymbol{q}_1}\delta^{(1)}_{\boldsymbol{q}_2}\delta_D(\boldsymbol{p}-\boldsymbol{q}-\boldsymbol{q}_1-\boldsymbol{q}_2), \qquad \text{(A.58)} \end{aligned}$$

where,

$$\beta_{ij}(\boldsymbol{q},\boldsymbol{p}) = \frac{(p_i-q_i)q_j - \frac{1}{3}\delta_{ij}(\boldsymbol{p}-\boldsymbol{q})\cdot\boldsymbol{q}}{(\boldsymbol{p}-\boldsymbol{q})^2q^2}, \text{and} \qquad \text{(A.59)}$$

$$\tilde{H}_2(\boldsymbol{q}_1,\boldsymbol{q}_2) = \frac{2}{5}G_2(\boldsymbol{q}_1,\boldsymbol{q}_2) + \frac{3}{5}F_2(\boldsymbol{q}_1,\boldsymbol{q}_2) = \frac{3}{5} + \frac{1}{2}\mu\left(\frac{q_1}{q_2}+\frac{q_2}{q_1}\right) + \frac{2}{5}\mu^2. \qquad \text{(A.60)}$$

Using the previous results, we can easily compute

$$\begin{aligned} \langle\delta_\ell\sigma_{\rm eff}\rangle &= \frac{1}{\bar{\rho}}\left\langle\delta^\ell_{\boldsymbol{k}}\frac{p_ip_j}{p^2}\left[\hat{\tau}^{(3)}_{ij}\right]^{\Lambda}_{\boldsymbol{p}}\right\rangle \\ &= -10\mathcal{H}^2W_\Lambda(k)\langle\delta^{(1)}_{\boldsymbol{k}}\delta^{(1)}_{\boldsymbol{p}}\rangle\int_{\boldsymbol{q}}\beta(\boldsymbol{q},-\boldsymbol{k})\tilde{H}_2(-\boldsymbol{k},\boldsymbol{k}+\boldsymbol{q})P_\delta(|\boldsymbol{p}-\boldsymbol{q}|), \\ &\quad + \mathcal{H}^2W_\Lambda(p)\int_{\boldsymbol{q}}\int_{\boldsymbol{q}_1}\int_{\boldsymbol{q}2}\frac{(\boldsymbol{p}\cdot\boldsymbol{q}_1)(\boldsymbol{p}\cdot\boldsymbol{q}_2) - \frac{1}{3}p^2\boldsymbol{q}_1\cdot\boldsymbol{q}_2}{p^2q_1^2q_2^2}\langle\delta^{(1)}_{\boldsymbol{k}}\delta^{(1)}_{\boldsymbol{p}-\boldsymbol{q}}\delta^{(1)}_{\boldsymbol{q}_1}\delta^{(1)}_{\boldsymbol{q}_2}\rangle\delta_D(\boldsymbol{q}-\boldsymbol{q}_1-\boldsymbol{q}_2) \qquad \text{(A.61)} \end{aligned}$$

$$= -10\mathcal{H}^2 W_\Lambda(k)\langle\delta^{(1)}_{\boldsymbol{k}}\delta^{(1)}_{\boldsymbol{p}}\rangle \int_{\boldsymbol{q}} \beta(\boldsymbol{q}-\boldsymbol{k},-\boldsymbol{k})\tilde{H}_2(-\boldsymbol{k},\boldsymbol{q})P_\delta(q),$$
$$- \mathcal{H}^2 W_\Lambda(p)\langle\delta^{(1)}_{\boldsymbol{k}}\delta^{(1)}_{\boldsymbol{p}}\rangle \int_{\boldsymbol{q}} \frac{1}{q^2} \underbrace{\left[\frac{1}{3} - \frac{q}{p}\mu - \mu^2\right]}_{=0 \text{ after angular integration}} P_\delta(q) \tag{A.62}$$

where

$$\beta(\boldsymbol{q},\boldsymbol{p}) \equiv \frac{p_i p_j}{p^2}\beta_{ij}(\boldsymbol{q},\boldsymbol{p}) = \frac{\boldsymbol{p}\cdot(\boldsymbol{p}-\boldsymbol{q})\boldsymbol{p}\cdot\boldsymbol{q} - \frac{1}{3}p^2(\boldsymbol{p}-\boldsymbol{q})\cdot\boldsymbol{q}}{p^2q^2(\boldsymbol{p}-\boldsymbol{q})^2} \tag{A.63}$$

and taking limits $k \ll q$

$$\begin{aligned}
&\beta(\boldsymbol{q}-\boldsymbol{k},-\boldsymbol{k})\tilde{H}_2(-\boldsymbol{k},\boldsymbol{q}) \\
&\qquad = -\frac{1}{q^2}\left[-\frac{1}{3} - \frac{4}{3}\mu\frac{k}{q} + \mu^2 + 2\mu^3\frac{k}{q}\right] \times \left[\frac{3}{5} - \frac{1}{2}\mu\frac{q}{k} + \frac{2}{5}\mu^2\right] \\
&\qquad = -\frac{1}{q^2}\left[-\frac{1}{5} + \frac{17}{15}\mu^2 - \frac{3}{5}\mu^4 + \mathcal{O}(k)\right] + \text{ terms of odd order in } \mu
\end{aligned} \tag{A.64}$$

and thus,

$$\begin{aligned}
c^2_{\rm sv} &\equiv \frac{\langle\delta_l\sigma_{\rm eff}\rangle}{\langle\delta_l\delta_l\rangle} = 10\mathcal{H}^2\frac{1}{(2\pi)^2}\int_{\boldsymbol{q}}\frac{1}{q^2}\left[-\frac{1}{5} + \frac{17}{15}\mu^2 - \frac{3}{5}\mu^4\right]P_\delta(q) \\
&= \frac{26}{45}\frac{1}{2\pi^2}\mathcal{H}^2\int \mathrm{d}q\, P_\delta(q),
\end{aligned} \tag{A.65}$$

$$c^2_{\rm comb} \equiv c^2_{\rm s} + c^2_{\rm bv} + c^2_{\rm sv} = \frac{61}{70}\frac{1}{2\pi^2}\mathcal{H}^2\int \mathrm{d}q\, P_\delta(q) \tag{A.66}$$

A.3 Divergences in P_{13}

By design of the EFTofLSS the UV-divergences in $P_{c_s^2}$ should be cancelled by the divergences in P_{13}. To check this, we want to compute P_{13} as well. We start with,

$$\begin{aligned}
\left\langle\delta^{(1)}_{\boldsymbol{k}}\delta^{(3)}_{\boldsymbol{p}}\right\rangle &= \int_{\boldsymbol{q}_1}\int_{\boldsymbol{q}_2}\int_{\boldsymbol{q}_3}\delta_D(\boldsymbol{p}-\boldsymbol{q}_1-\boldsymbol{q}_2-\boldsymbol{q}_3)F_3(\boldsymbol{q}_1,\boldsymbol{q}_2,\boldsymbol{q}_3)\left\langle\delta^{(1)}_{\boldsymbol{k}}\delta^{(1)}_{\boldsymbol{q}_1}\delta^{(1)}_{\boldsymbol{q}_2}\delta^{(1)}_{\boldsymbol{q}_3}\right\rangle \\
&= 3\int_{\boldsymbol{q}_1}\int_{\boldsymbol{q}_2}F_3^{(\rm s)}(\boldsymbol{q}_1,\boldsymbol{q}_2,\boldsymbol{p}-\boldsymbol{q}_1-\boldsymbol{q}_2)\left\langle\delta^{(1)}_{\boldsymbol{k}}\delta^{(1)}_{\boldsymbol{p}-\boldsymbol{q}_1-\boldsymbol{q}_2}\right\rangle\left\langle\delta^{(1)}_{\boldsymbol{q}_1}\delta^{(1)}_{\boldsymbol{q}_2}\right\rangle \\
&= 3\delta_D(\boldsymbol{k}+\boldsymbol{p})P_\delta(k)\int_{\boldsymbol{q}}P_\delta(q)F_3^{(\rm s)}(\boldsymbol{k},\boldsymbol{q},-\boldsymbol{q})
\end{aligned} \tag{A.67}$$

from which we get the power spectrum

$$\begin{aligned}
P_{13}(k) &= 6P_\delta(k)\int_{\boldsymbol{q}}P_\delta(q)F_3(\boldsymbol{k},\boldsymbol{q},-\boldsymbol{q}) \\
&= 6P_\delta(k)\frac{k^3}{(2\pi)^2}\int_0^{k_c/k}\mathrm{d}r\, P_\delta(kr)\int_{-1}^{1}\mathrm{d}\mu\, r^2F_3(\boldsymbol{k},\boldsymbol{q},-\boldsymbol{q}),
\end{aligned}$$

where in the last line we split the integral in a radial and a angular component and wrote $r = q/k$. We want to look at the large r limit, *i.e.* $k \ll q$, so we want F_3 up to $\mathcal{O}\left(\frac{1}{r^2}\right)$ and only the terms with even powers in μ. We use equation (A.4) from [3] for the divergent part

of F_3,

$$\begin{aligned}
F_3(\boldsymbol{k},\boldsymbol{q},-\boldsymbol{q}) &= \frac{1}{q^2+k^2-2\boldsymbol{k}\cdot\boldsymbol{q}}\left[\frac{5k^2}{126}-\frac{11\boldsymbol{k}\cdot\boldsymbol{q}}{108}+\frac{7(\boldsymbol{k}\cdot\boldsymbol{q})^2}{108k^2}-\frac{k^2(\boldsymbol{k}\cdot\boldsymbol{q})^2}{54q^4}+\frac{4(\boldsymbol{k}\cdot\boldsymbol{q})^3}{189q^4}-\frac{23k^2\boldsymbol{k}\cdot\boldsymbol{q}}{756q^2}\right.\\
&\quad\left.+\frac{25(\boldsymbol{k}\cdot\boldsymbol{q})^2}{252q^2}-\frac{2(\boldsymbol{k}\cdot\boldsymbol{q})^3}{27k^2q^2}\right]\\
&\quad+\frac{1}{q^2+k^2+2\boldsymbol{k}\cdot\boldsymbol{q}}\left[\frac{5k^2}{126}+\frac{11\boldsymbol{k}\cdot\boldsymbol{q}}{108}-\frac{7(\boldsymbol{k}\cdot\boldsymbol{q})^2}{108k^2}-\frac{4k^2(\boldsymbol{k}\cdot\boldsymbol{q})^2}{27q^4}-\frac{53(\boldsymbol{k}\cdot\boldsymbol{q})^3}{189q^4}+\frac{23k^2\boldsymbol{k}\cdot\boldsymbol{q}}{756q^2}\right.\\
&\quad\left.-\frac{121(\boldsymbol{k}\cdot\boldsymbol{q})^2}{756q^2}-\frac{5(\boldsymbol{k}\cdot\boldsymbol{q})^3}{27k^2q^2}\right]\\
&= \frac{1}{1+\frac{1}{r^2}-2\frac{\mu}{r}}\left[\frac{5}{126r^2}-\frac{11\mu}{108r}+\frac{7\mu^2}{108}+\frac{25\mu^2}{252r^2}-\frac{2\mu^3}{27r}+\mathcal{O}\left(\frac{1}{r^3}\right)\right]\\
&\quad+\frac{1}{1+\frac{1}{r^2}+2\frac{\mu}{r}}\left[\frac{5}{126r^2}+\frac{11\mu}{108r}-\frac{7\mu^2}{108}-\frac{121\mu^2}{756r^2}-\frac{5\mu^3}{27r}+\mathcal{O}\left(\frac{1}{r^3}\right)\right]\\
&= \left[1+2\frac{\mu}{r}+\frac{4\mu^2-1}{r^2}+\mathcal{O}\left(\frac{1}{r^3}\right)\right]\left[\frac{7\mu^2}{108}-\frac{11\mu+8\mu^3}{108r}+\frac{10+25\mu^2}{252r^2}+\mathcal{O}\left(\frac{1}{r^3}\right)\right]\\
&\quad+\left[1-2\frac{\mu}{r}+\frac{4\mu^2-1}{r^2}+\mathcal{O}\left(\frac{1}{r^3}\right)\right]\left[-\frac{7\mu^2}{108}+\frac{11\mu-20\mu^3}{108r}+\frac{30-121\mu^2}{756r^2}+\mathcal{O}\left(\frac{1}{r^3}\right)\right]\\
&= \frac{5}{63r^2}-\frac{59\mu^2}{126r^2}+\frac{2\mu^4}{9r^2}+\mathcal{O}\left(\frac{1}{r^3}\right)
\end{aligned}$$

and thus, for a linear power spectrum $P_\delta(k)=Aa^2k^n$ with $n\geq 0$,

$$P_{13}(k) = 6A^2a^4\frac{k^{3+n}}{(2\pi)^2}\int_0^{k_c/k}\mathrm{d}r\,(kr)^n\int_{-1}^{1}\mathrm{d}\mu\,\left[\frac{5}{63}-\frac{59\mu^2}{126}+\frac{2\mu^4}{9}\right] \tag{A.68}$$

$$= 6A^2a^4\frac{k^{3+n}}{(2\pi)^2}\frac{k^n(k_c/k)^{n+1}}{n+1}\left(-\frac{61}{945}\right) \tag{A.69}$$

$$= -\frac{244}{315(n+1)}A^2a^4\pi\frac{k^{2+n}k_c^{n+1}}{(2\pi)^3}, \tag{A.70}$$

where k_c is the UV-cutoff.

Bibliography

[1] F. Bernardeau, S. Colombi, E. Gaztanaga, and R. Scoccimarro, "Large-scale structure of the universe and cosmological perturbation theory," *Physics Reports* **367** no. 1, (2002) 1–248, arXiv:astro-ph/0112551.

[2] R. Takahashi, "Third-order density perturbation and one-loop power spectrum in dark-energy-dominated universe," *Progress of Theoretical Physics* **120** no. 3, (2008) 549–559, arXiv:0806.1437 [astro-ph].

[3] E. Pajer and M. Zaldarriaga, "On the renormalization of the effective field theory of large scale structures," *Journal of Cosmology and Astroparticle Physics* **2013** no. 08, (2013) 037, arXiv:1301.7182 [astro-ph].

[4] W. J. Percival, "Large scale structure observations," arXiv:1312.5490 [astro-ph].

[5] "The 2df galaxy redshift survey." http://www.2dfgrs.net/.

[6] "Sloan digital sky survey legacy." http://classic.sdss.org/signature.html.

[7] D. Baumann, A. Nicolis, L. Senatore, and M. Zaldarriaga, "Cosmological non-linearities as an effective fluid," *Journal of Cosmology and Astroparticle Physics* **2012** no. 07, (2012) 051, arXiv:1004.2488 [astro-ph].

[8] O. Lahav and Y. Suto, "Measuring our universe from galaxy redshift surveys," *Living Reviews in Relativity* **7** no. 8, (2004) . http://www.livingreviews.org/lrr-2004-8.

[9] J. J. M. Carrasco, M. P. Hertzberg, and L. Senatore, "The effective field theory of cosmological large scale structures," *Journal of High Energy Physics* **2012** no. 9, (2012) 1–40, arXiv:1206.2926 [astro-ph].

[10] S. Engineer, N. Kanekar, and T. Padmanabhan, "Non-linear density evolution from an improved spherical collapse model," *Monthly Notices of the Royal Astronomical Society* **314** no. 2, (2000) 279–289.

[11] P. Fosalba and E. Gaztanaga, "Cosmological perturbation theory and the spherical collapse modeli. gaussian initial conditions," *Monthly Notices of the Royal Astronomical Society* **301** no. 2, (1998) 503–523.

[12] L. Mercolli and E. Pajer, "On the velocity in the effective field theory of large scale structures," *Journal of Cosmology and Astroparticle Physics* **2014** no. 03, (2014) 006, arXiv:1307.3220.

[13] T. Padmanabhan and S. Engineer, "Nonlinear gravitational clustering: Dreams of a paradigm," *The Astrophysical Journal* **493** no. 2, (1998) 509, 9704224 [astro-ph].